HERA machine studies December 1998

M. Bieler, E. Gianfelice-Wendt, G. H. Hoffstätter, B. Holzer,
C. Kleffner, T. Limberg, Ch. Montag, A. Meseck, M. Seidel,
F. Solodovnik, M. Wendt, F. Willeke, K. Wittenburg

March 1999

Edited by G. H. Hoffstätter

Contents

Abstract

The machine studies at the HERA accelerator performed during December 1998 were mainly related to the luminosity upgrade project. In parallel to this project the electron beam current should be brought up to 56mA. This brings about two problems. Firstly the lifetime at pressent drops strongly when currents of more than around 35mA are stored and secondly, so far we do not know what effects such high electron currents will have on the proton beam during many hours of luminosity operation. Studies were performed to obtain insight into both problems. To attain these high electron currents in HERA the efficacy of the injection process has to be optimized, and an orbital coupling effect observed during injection was therefore analyzed. It is also planned to increase the proton currents and therefore a tool for optimizing the transport of protons from PETRA to HERA was commissioned during this machine study period.

Along with a current increase, the emittance of the electron beam has to be reduced from 41πnm to 22πnm. It is intended to achieve this by two means: stronger focusing in the arcs and increasing the RF frequency. Therefore, the emittance and the central frequency were measured by various methods, and the two means of emittance reduction were tested in the present HERA electron ring.

In addition to these studies, which are strongly related to the luminosity upgrade project, two studies of general proton ring improvement were performed. The possibility of microwave instabilities in HERA-p was analyzed and a method of measuring chromaticity during the ramp with little emittance dilution was tested with encouraging results.

Last but not least, the severe background due to a coasting proton beam was analyzed and a method for increasing the population of the proton tails for the HERA-B experiment was investigated.

1 Current Dependent Orbit Distortion and Beam-Lifetime Reduction in HERA-e

Date: 1998, Dec. 16, 11pm to Dec. 17, 3pm Logbook XXXIV, page 157–168

This report describes observations in normal runs as well as dedicated experiments in HERA, 1998. During some luminosity runs it had been observed that the beam orbit in the electron machine changes with time by considerable amounts. In parallel lifetime reductions were observed and in some cases it could be suspected that those happened in connection with the orbit movements, due to aperture limits or so. The orbit motion results in the necessity to tune up luminosity from time to time and is at least unpleasant. However, the lifetime reduction which is sometimes dramatic, is a serious problem, and if it is caused (at least partially) by the orbit motion, this effect should be understood and removed. Dedicated experiments were done on October 10'th, and December 16'th.

1.1 Codes and Numerical Tools

In order to provide data with high time resolution a simple Visual Basic application has been written which allows to store electron orbits at a maximum rate of 1 Hz on disc. The program can be found under

`S:\Projects\Vb\Orbcor\Test\Project1.exe` ,

and the data files are stored under `S:\tempdata\e_orbits\` . The regular data files have names like `d12_170853.dat` , where 12 is the day of the month and the other 6 digits give the time when the file was written. The files contain 277 x and y orbit positions of the beam, and current as well as lifetime in the last line. Everybody is welcome to use this program for other purposes, but don't forget to switch it off after usage and clean up the data folder from time to time!

After a run of several hours and typical orbit-writing-rates of 0.1 Hz several hundred orbits have been measured and are written to disc. The question arises how one can take advantage of such a large amount of data, especially in view of the suppression of statistical errors. If noticeable orbit movements are recorded it is important to decide whether there is only one underlying process that originates the orbit distortion, or if there are several independent effects. Under the keyword "Model Independent Analysis (MIA)" one can find a numerical method in the literature that attempts to attack these two questions[1]. The method is based on Singular Value Decomposition (SVD) of the orbit matrix. An orbit matrix $\mathbf{B}$ is built up of individually measured orbit vectors by arranging them in rows. In other words, the column index of $\mathbf{B}$ is a spatial index, it describes the location in the ring, whereas the row index is the number of the measurement, a time variable

[1] Y.T. Yan et al., EPAC 1998, `http://www.cern.ch/accelconf/e98/PAPERS/WEP21G.PDF`

(if measuring intervals are equidistant). The SVD of this matrix results in three matrices, two orthogonal ones ($\mathbf{U}, \mathbf{V}$), and a diagonal one, $\mathbf{\Lambda}$.

$$\mathbf{B} \quad = \quad \mathbf{U\Lambda V^T}$$

$$\text{with :} \quad \begin{array}{rcl} \mathbf{U^T} & = & \mathbf{U^{-1}} \\ \mathbf{V^T} & = & \mathbf{V^{-1}} \end{array} \quad \text{, and} \quad \mathbf{\Lambda} = \begin{bmatrix} \lambda_1 & 0 & . \\ 0 & \lambda_2 & . \\ . & . & \lambda_n \end{bmatrix}$$

The orbit motion is thereby decomposited into a set of normalized spatial vectors (orbit patterns) in matrix $\mathbf{V}$, and a set of temporal vectors that describe the time development in matrix $\mathbf{U}$. The diagonal matrix $\mathbf{\Lambda}$ contains rms orbit variations, averaged both over the measurement time and the spatial distribution around the ring. Each number in $\mathbf{\Lambda}$ corresponds to one temporal vector and one spatial vector[2].

The key of the method is now that only a limited number of underlying physical processes result in orbit motions, i.e. the 277 beam position monitors (BPM's) in HERA will in general not vary independently, but according to certain correlation laws, as for instance a betatron orbit oscillation. The limited number of degrees of freedom in the system is reflected by the fact that only a small number of eigenvalues in $\mathbf{\Lambda}$ will have a large magnitude, and consequently only the corresponding temporal and spatial eigenvectors are relevant.

Our application of the described SVD method is to find out whether we can relate the observed HERA-e orbit motions to a single underlying effect or if there are several effects with possibly different behaviors vs. time. The number of significantly valued λ_i should answer this question.

1.2 Observations of Orbit Motions

During two dedicated experimental shifts, on October 14'th and December 17'th, the orbit motion was observed without collisions, with relatively high currents and without affecting the machine otherwise. The measurements where performed at 27 GeV with starting currents of 28 mA and 36 mA respectively. Spatially averaged rms orbit variations over times of two or three hours amount to 1.2 mm or more. In both cases only one major effect is causing the orbit distortion. Fig. 1 shows as an example the first largest eigenvalues from the SVD of the BPM matrix (measurement 14/10/98). The first temporal vector, scaled by the rms-value (1'st eigenvalue) shows the spatially averaged rms orbit deviation as a function of time. The curve exhibits a steep change in the beginning, saturates then, and decays later similar as the beam current. This is especially obvious when a part of the beam is kicked out (see Fig 3).

Knowing that only one process plays a role we would like to find out what it is and where it is located. The spatial vector corresponding to the largest eigenvalue looks like a betatron orbit oscillation, so one tries first to explain it by a single orbit kick. Indeed the pattern can be fit successfully by applying one most effective corrector, as is demonstrated by Fig. 2.

[2]Sometimes one talks about eigenvalues and eigenvectors here. The connection is that $\mathbf{V}$ contains the eigenvectors of the matrix $(\mathbf{B^T B})$ and $\mathbf{\Lambda}$ contains the square-roots of their eigenvalues. Similar $\mathbf{U}$ for $(\mathbf{BB^T})$.

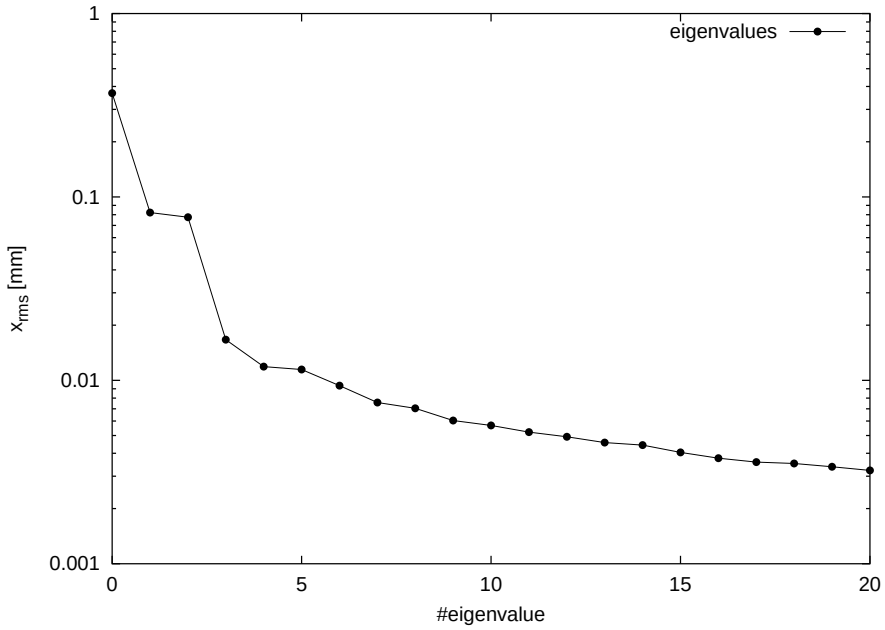

Figure 1: Magnitude of the first eigenvalues showing that one process is dominating the orbit motion. The second eigenvalue is already smaller than the first one by a factor 4.

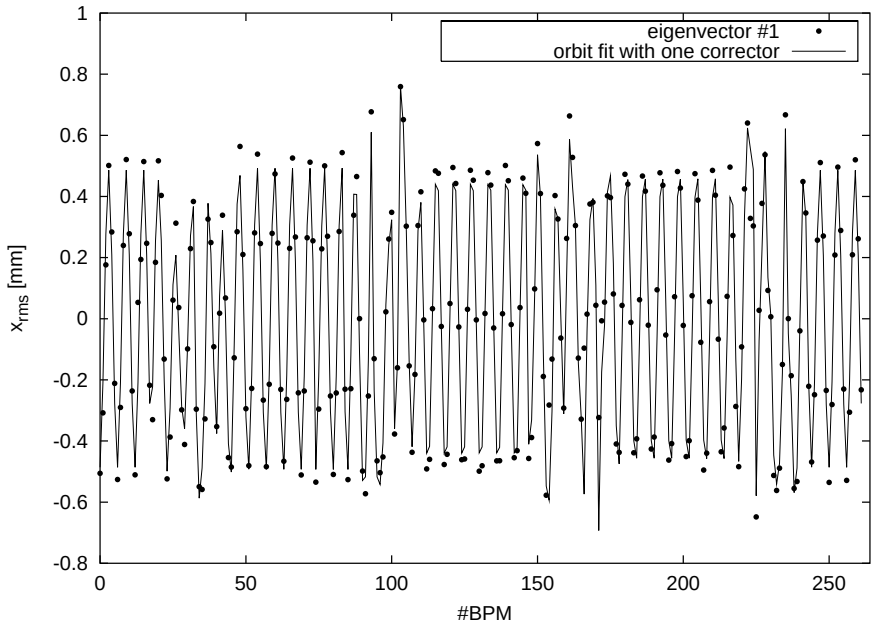

Figure 2: Spatial eigenvector #1 and a fitted orbit, generated by one most effective corrector. The amplitude is scaled by the corresponding rms value in $\mathbf{\Lambda}$.

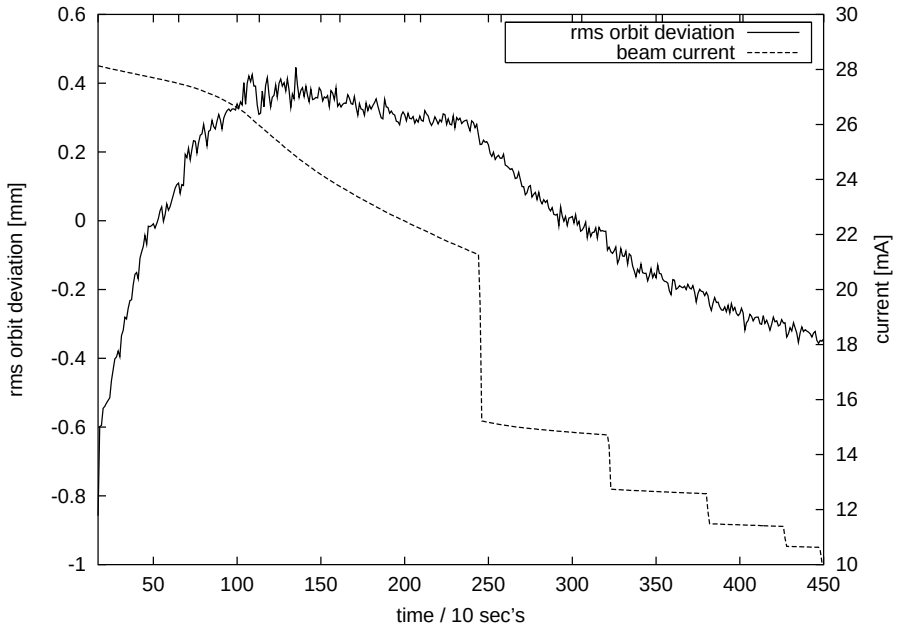

Figure 3: Temporal behaviour.

The location of the most effective corrector lies in the interaction region south. In order to find the position precisely one can compute the rms deviation of the best fit from the spatial vector as a function of the corrector position in betatron phase. In other words, a virtual corrector dipole is placed in fine steps at all possible phases and then varied in strength such as to fit the measured orbit best. The quality of the corrector position is evaluated by computing the rms deviation from the measured orbit. The real position of the kick should be found at the minimum of this curve. Of course the curve exhibits typically similar minima at π phase differences. Unfortunately, during the first measurement, the two monitors SL7 and SR7 which seem to be very close to the kick, did not work correctly. This results in four nearly equal lowest minima of the RMS deviation curve, which prevents the clear identification of the kick. During the second measurement the above mentioned monitors worked correctly. The curve is shown in Fig. 4. It still exhibits two equal minima which are located very close to the IP, on the left side. The described method suffers from the fact that, due to the large number of monitors, the difference of placing the kick between two monitors or the next two monitors is relatively small. Therefore we tried a different scheme by fitting only a piece of the spatial vector (typ. 10 monitors) and then shifting this piece monitor by monitor. The betatron oscillation should exhibit a phase jump at the location of the kick and this jump should become obvious by the piecewise fit. Fig. 5 shows three piecewise fitted curves, one left of the IP, one centered around the IP and one right from the IP. Indeed one finds the phases of the curves to shift gradually while crossing over the IP. Unfortunately the two monitors at 7 m from the IP (left and right) do not match one or the other curve better.

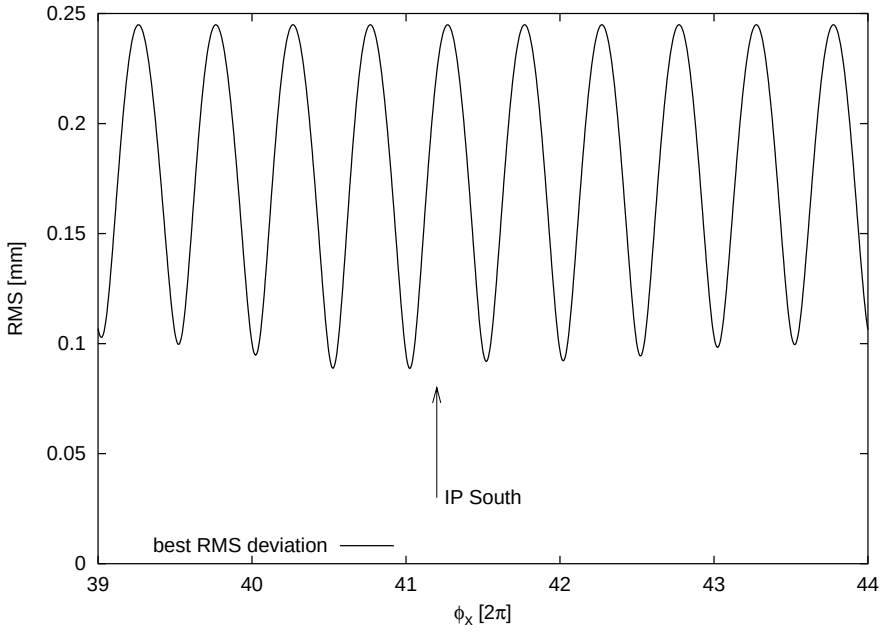

Figure 4: RMS deviation of the fitted orbit to the measured one as a function of the corrector position.

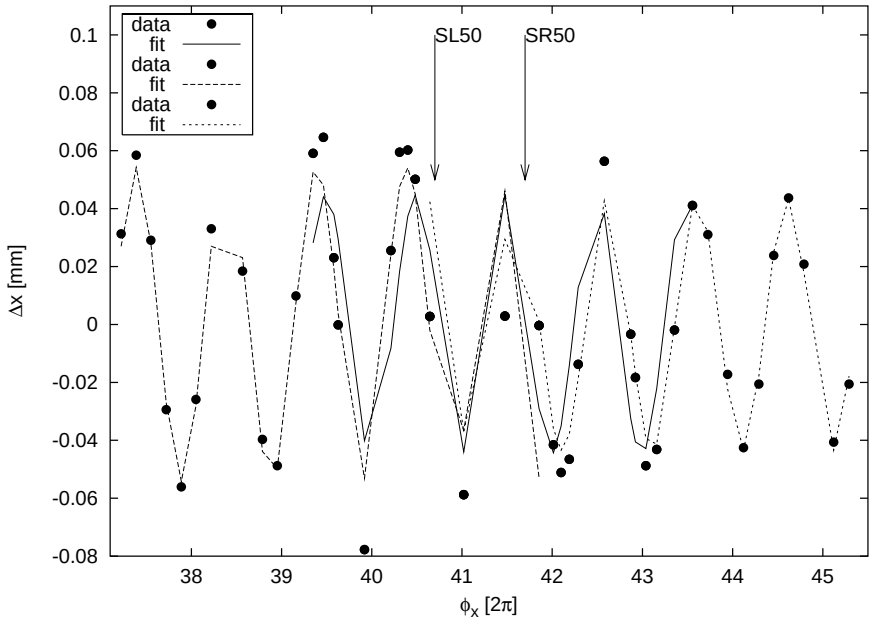

Figure 5: Piecewise fit.

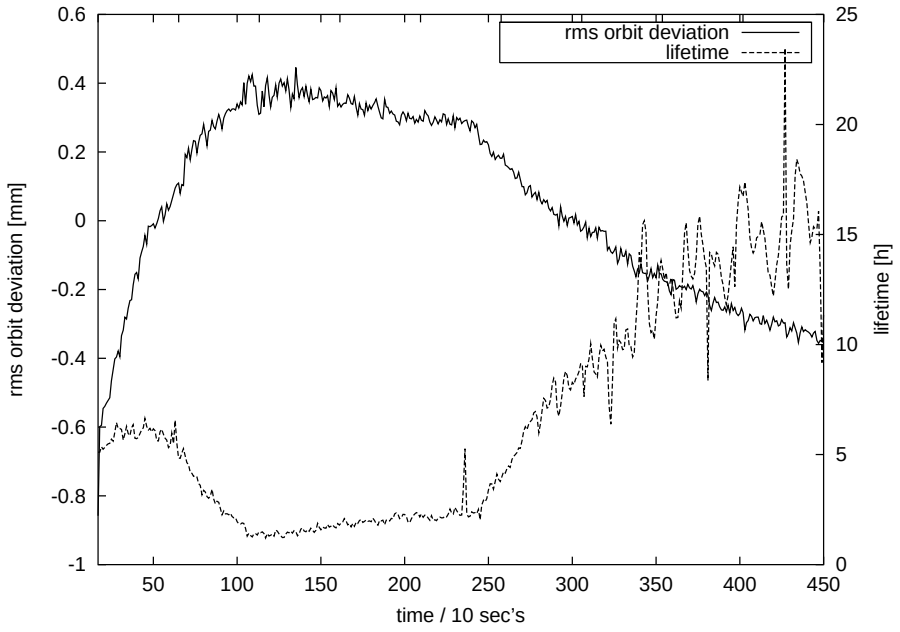

Figure 6: Lifetime and orbit-distortion during measurement 1.

1.3 Orbit Motion and Beam Lifetime

During normal operation and also during our first dedicated measurement rather dramatic beam lifetime reductions were observed, that went away after a wile with decaying beam currents. On the other hand, in other cases with very large currents, lifetime reductions occurred which did not vanish with decaying current. Those events look like "dust"-events, well known from the pre-NEG pump era. Fig. 6 shows the orbit distortion amplitude together with the beam lifetime vs. time for the first measurement (10/10/98). At the end of the ramp the lifetime was relatively good with 5 hours at 28 mA. But after about 10 minutes it started to decrease and reached its minimum exactly when the orbit amplitude reached the maximum. This coincidence makes it likely that the orbit motion causes the lifetime reduction, at least in this case.

In the second measurement a poor lifetime of about 1 hour was observed as well (Fig. 7). However, this time the lifetime was poor already from the beginning on, and it did not recover to a level of more than 10 hours as in the first measurement. The amplitude of the orbit distortion was even slightly larger than for the other case. Nevertheless there is no correlation between lifetime and orbit amplitude.

In order to find out what caused the lifetime reduction in the first case, the orbit distortion was artificially introduced by turning on a correction coil that most effectively corrects the observed orbit oscillation (SL61 CH). Surprisingly the effect of the kick is rather asymmetric. Turning the coil to one direction leads to a sudden beam loss at a certain amplitude, as one would expect from an aperture limit. However, the other polarity leads to a slow reduction of the lifetime with no sharp boundary. At an rms amplitude of the orbit distortion of ≈ 1.7 mm the lifetime was reduced from 2.5 hours to 1 hour. At the same time an increase of the horizontal beam width was observed on the synchrotron radiation (SR) monitor. This could be interpreted as a modification of the damping distribution of the

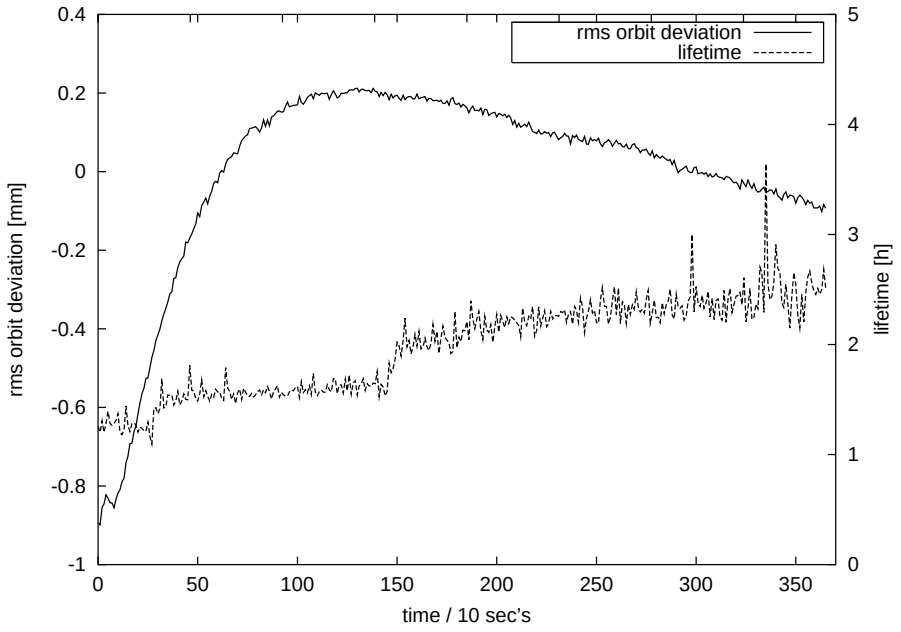

Figure 7: Lifetime and orbit-distortion during measurement 2.

machine, resulting in a larger emittance, which in turn would explain the smooth lifetime reduction. Note that the 1.7 mm amplitude is not very far from the natural orbit amplitudes, produced by the thermal effect. In order to support this theory a MAD simulation on the impact of a closed orbit distortion by the corrector SL61CH on the damping distribution has been performed (G. Hoffstätter). The result is shown in Fig. 8. It turns out that this kick actually decreases the horizontal emittance. At the same time the energy spread is increased. Since the SR monitor is located at a dispersive position the visible spotsize is a quadratic sum of the beamsize caused by emittance and by energy spread. Unfortunately the two effects cancel roughly, such that the redistribution of the damping partitions would not be visible on the monitor, in contradiction to our observations in the machine.

1.4 Summary

Significant orbit movements can be observed in HERA-e at higher beam currents. The rms value (averaged over monitors) of the orbit variation changes typically by 1 mm over periods of one or two hours. From an SVD analysis of the orbit data we conclude that only one underlying effect is causing the orbit motion. The shape of orbit amplitude versus time suggests a thermal effect. Supposed that a beampipe would heat up by SR or higher order mode (HOM) losses, would bow and take a quadrupole with it, this would explain a beam current dependent orbit kick. In order to explain the observed magnitudes a quadrupole of typical strength would have to move by $\approx 300\,\mu$m. At DORIS such effects are well known and observed orbit amplitudes look qualitatively exactly like ours. Concerning the location of the kick it seems clear that it lies in the IR south. Precise location is difficult with the given data. The best strategy to find the location is probably to equip one by one quadrupole with position sensors and to detect magnet motions directly.

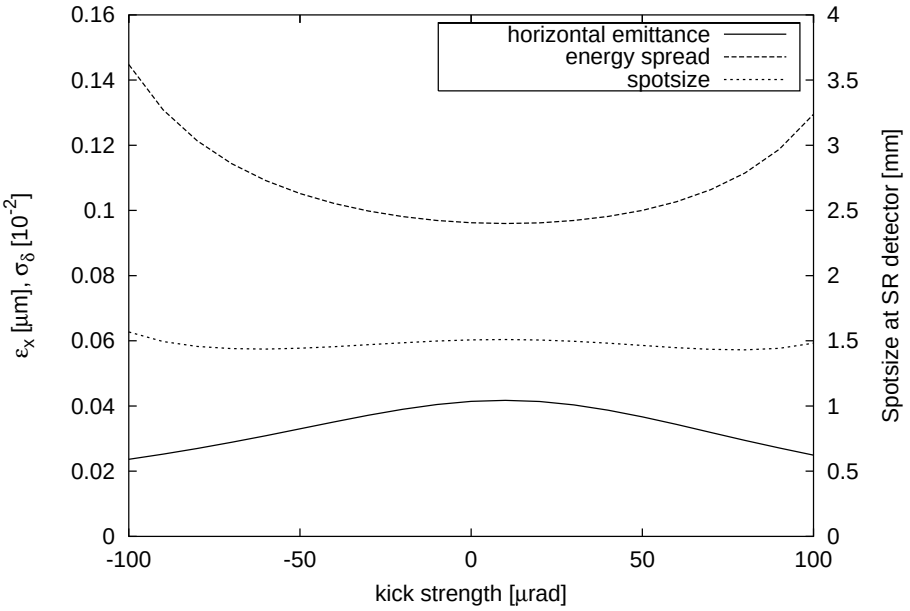

Figure 8: Horizontal emittance, energy spread and predicted spot size at the SR monitor.

Concerning orbit correlated lifetime reductions we are probably suffering from two distinct effects. One are the traditional HERA-e lifetime problems that exhibit a strong memory effect and are independent of the beam orbit. The other class can be caused by orbit distortions, not unlikely distortions of the magnitude typically observed in normal runs. A possible explanation of the weak dependence of the lifetime on an artificially introduced orbit distortion is a redistribution of the damping partitions. However, the observed change of the beam spotsize on a SR monitor could not be reproduced by a MAD simulation.

2 Experiences with a 72° HERA-e Optics

Date: 1998, Dec. 17, 3pm to Dec. 20, 11pm, Logbook XXXIV, page 177–202

In the HERA luminosity upgrade the horizontal emittance of the electron beam has to be reduced from currently 41πnm to 22πnm [5]. Part of the reduction will be achieved by increasing the RF frequency as discussed in section 4. The RF frequency shift alone, without an increased focusing can however not be used, since this would lead to an increased longitudinal emittance which then would lead to a loss in longitudinal lifetime if the RF system is not changed. Therefore a shift in the RF frequency is only possible when an increased focusing in the FODO cells has been used to reduce the momentum compaction α_p and thereby to increase the bucket height. This makes space for an increased longitudinal emittance without a change of the RF system. We analyzed several possible optics for the luminosity upgrade lattice with various phase advances in the horizontal and vertical plane of the FODO cells [1]. A lattice with 72° phase advance per FODO cell in both planes turned out to be most promising because it had the most acceptable dynamic aperture. Without an RF frequency shift, the electron beam in such a lattice has an emittance of 27πmm·mrad at 27.5GeV. The stronger focusing gives space for 200Hz increase in frequency which further reduces the emittance to 22πmm·mrad. The energy decrease going along with such a frequency shift is only -0.083% .

To test the usability of such an optics in the upgraded HERA-e, a 72° optic was installed in the current ring, which leads to a simulated horizontal emittance of 34πnm. The dynamic aperture of this optics was measured and compared to measurements of the dynamic aperture for the current 60° optics.

2.1 Introduction

In the HERA-e ring two optic files are required to accelerate electrons from 12GeV to 27.5GeV; an injection optic file and a luminosity optic file.

A new luminosity file with 72° focusing at 27.5GeV has been produced by taking the current optics in the interaction region and the periodic optic in the 72° FODO cells and match the dispersion and the beta function of the two regions together. This is done using quadrupoles of the matching regions which are symmetric to the right and left of the straight sections. The procedure is rather straight forward and good matches could be computed easily in the symmetric South and North regions. In the West section also each power-supply serves two magnets, one to the right and one to the left of the center region. However, here the magnets are not arranged symmetrically. It is therefore somewhat harder to match the left and

the right part simultaneously with symmetric currents but non-symmetric magnet arrangements, nevertheless good matches were possible.

The injection file has larger beta functions in the interaction regions. The optics in these regions has again been taken from the current injection file and has been matched to the periodic arcs with 72° FODO cells by adjusting quadrupoles in the matching sections. Special caution had to be taken in the West region, since the injection bump and the injection kickers are located within the matching section. Nevertheless the beta functions at and the phase advances between kickers were kept at their current value in order to keep the current kicker strength. When matching the new FODO cells with 72° to the West straight sections, therefore not only the matching conditions between arc and West central region had to be satisfied but additionally the beta function in the interaction region had to stay invariant [9].

The sextupoles in the luminosity optics and in the injection optics were used in two families to correct the chromaticities. Since the current six family scheme is designed for a 60° optics, no chromatic correction of optical functions was performed in the 72° case.

After electrons have been injected into the injection optics, the beam momentum and all magnetic fields are increased simultaneously to 27.5GeV. This leaves the optics unchanged. Then all magnetic fields are linearly interpolated between the injection optics and the luminosity optics keeping the beam's energy unchanged.

Both optic files have periodic beta and dispersion functions in the arcs. But when the fields are linearly interpolated, in general non symmetric arcs are produced. In fact, the first luminosity optics which was tested interpolated so badly with the injection optic that a very strong dispersion beat was produced. The dispersion was partially negative in the arcs and the beam became unstable while a large synchrotron spot size indicated anti-damping of the beam after 1/3 of the luminosity fields were reached during interpolation.

The problem was solved by computing a new luminosity optics for which the west straight section in the injection and in the luminosity file had the same optic function. The worst optics condition created during interpolation of the injection optics with this improved luminosity optics is shown in figure 9. After this change the interpolation could be performed without beam loss.

With this file arrangements injection, accumulation, ramp, and installing the luminosity file and luminosity tunes of Qx=52.148 and Qy=52.216 was unproblematic. The usual lifetime of around 15 hours at low currents (15mA) could be achieved and the orbit could be corrected to a usual rms of 1.22mm horizontally and 0.98 vertically. For this condition the dynamic aperture was then measured and compared with old measurements for the current 60° luminosity optics.

2.2 Measurement of dynamic aperture

When the beam is kicked by an angle Θ, the central particles travel with a Courant Snyder invariant $\beta_k\Theta^2$, with the beta function β_k at the kicker. When the central particles are kicked to a Courant Snyder invariant which corresponds to the dynamic aperture DA, then approximately half of the beam distribution will be outside the dynamic aperture and half will be inside. Therefore, the beam was kicked with the fourth injection kicker to various amplitudes and the relative beam loss

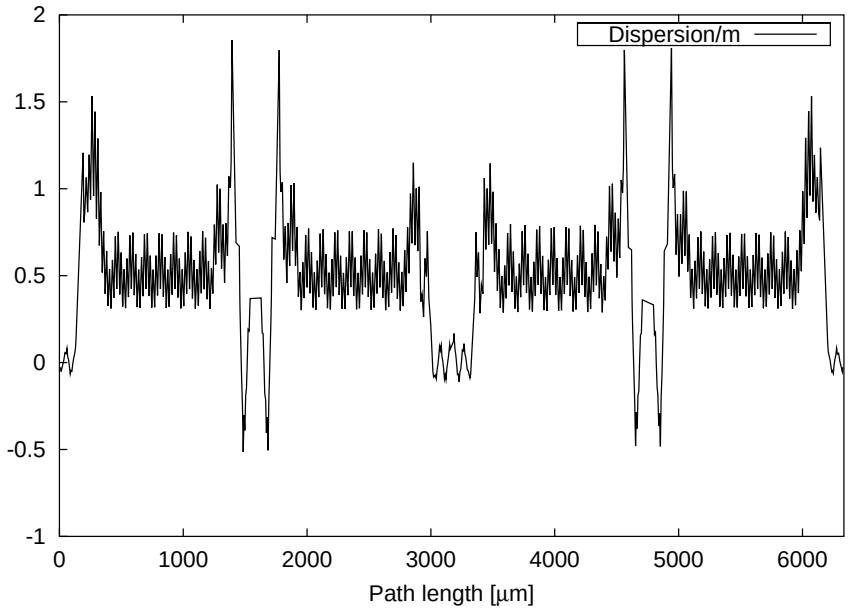

Figure 9: Strongest dispersion beat created when interpolating between the 72° injection optics and the 72° luminosity optics.

was measured. The voltage of kicker 4 and the resulting beam current reduction are shown in the figure 10 for the new 72° optics and in figure 11 for the current 60° optics. These data points were now interpolated to extrapolate the kicker voltage V_2 at which half the beam is lost. The corresponding kick Θ_2 and the dynamic aperture DA are then computed by

$$\Theta_2 = \frac{V_2}{\mathrm{kA}} \cdot 0.116\mathrm{mrad}\ , \quad DA = \beta_k \Theta_2^2\ , \quad DA_{rel} = \sqrt{\frac{DA}{\varepsilon}}\ . \tag{1}$$

For the 60° optics the beta function at the kicker is $\beta_k = 27$m and for the 72° optics we had $\beta_k = 34$m. The relative dynamic aperture DA_{rel} is an even more relevant quantity, since it describes how many sigma of the beam distribution fit into the dynamic aperture. The measurements shown in the figures 10 and 11 lead to the following dynamic apertures at 27.5GeV:

Optics	Date	V_2	DA	DA_{rel}
72° luminosity	20.Dec.1998	2.42 kV	2.7πmm·mrad	8.5σ
72° ramp file	20.Dec.1998	2.41 kV	2.6πmm·mrad	8.1σ
60° luminosity	14.Oct.1998	2.67 kV	2.6πmm·mrad	7.9σ
60° luminosity	14.Oct.1998	2.44 kV	2.2πmm·mrad	7.2σ
60° luminosity	17.Dec.1998	2.52 kV	2.3πmm·mrad	7.4σ
60° luminosity	17.Dec.1998	2.57 kV	2.4πmm·mrad	7.6σ

On average the dynamic aperture was 7.5σ with the current 60° optics; with the 72° optics the average was 8.3σ. Computationally the dynamic aperture of the new optic should be slightly smaller, since the sextupoles are excited more strongly to compensate for the larger natural chromaticity going along with stronger focusing. The fact that the dynamic aperture did not decrease when installing the new optics confirms the applicability of a 72° optics in the luminosity upgrade. Since these

studies, shortages to ground were found in three magnets. The repair of these shortages increased the injection efficiency strongly and most likely the dynamic aperture has also increased, future measurements will show by how much.

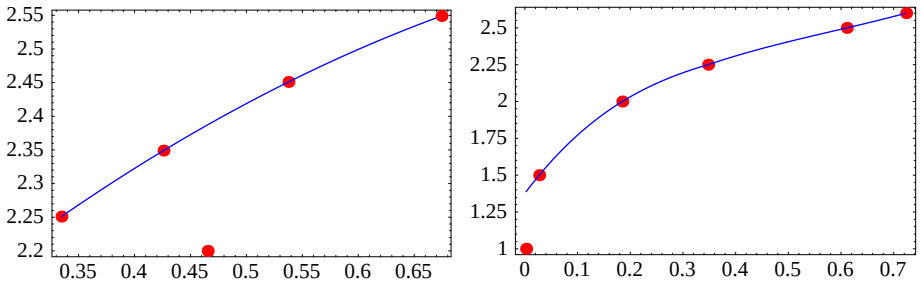

Figure 10: Kicker voltage as a function of the fraction of particles that are kicked out of the beam in the 72° optics.

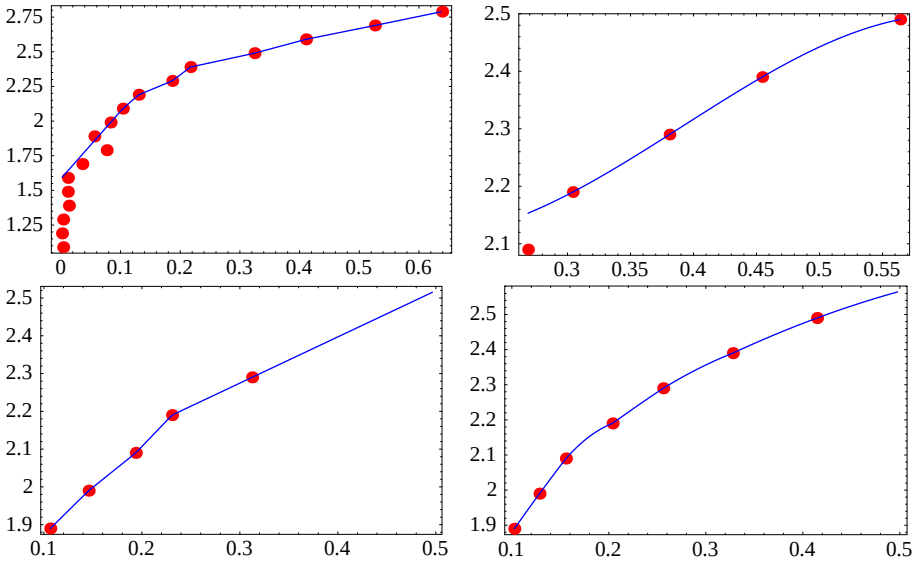

Figure 11: Kicker voltage as a function of the fraction of particles that are kicked out of the beam in the 60° optics. (These data were taken by B. Holzer, Logbook XXXIII page 45–47 and Logbook XXXIV page 169–173

3 The Emittance Measurements at the HERA Electron Ring with and without Beam–Beam Interaction

Date: 1998, Dec. 14, 6pm to Dec. 15, 11am Logbook XXXIV, page 139–144

3.1 Introduction

In order to protect the H1(and the ZEUS) detector from the synchrotron radiation caused by the electron beam, the knowledge of the transverse dimension of the radiation fan (at the IP) is necessary. The transverse dimension of the synchrotron radiation fan depends on the transverse dimension of the electron distribution and on the tails of the distribution in particular.

If the electron distribution is Gaussian, the measurements of the transverse standard widths σ_x and σ_y allow to determine the transverse electron emittances ϵ_x and ϵ_y.

With regard to the lumi-upgrade project the measurements of the transverse electron distribution with and without beam-beam interaction were carried out in the last machine studies.

The transverse electron distribution are measured by scraping the electron beam on the beam pipe. For this aim horizontal and vertical orbit bumps are excited and the beam lifetime is measured as a function of the current of the bump magnets.

3.2 Measurements

The measurements were made on December 14th, 15th in 1998.

The measurements were carried out in two cases. In the first case the magnets of the proton ring were put to lumi-condition but no protons were filled. So there was no beam-beam interaction. The horizontal and vertical emittances were measured. In the second case there was normal lumi-operation with a proton current of $60mA$. Only the horizontal emittance was measured in this case.

During the measurements the electron tune controller and the longitudinal feedback were switched on and the electron beam had an energy of 27.5 GeV and a beam current of 10 mA. The orbit bump had to be closed very well. If necessary, the bump was closed during the measurements.

The measurements were taken with two orbit bumps each time. The first bump, which was excited by three bump magnets, was supported by a second bump, which was excited by four bump magnets. This procedure made it possible to scrape the beam on the beam pipe and in addition to avoid the region where the magnetic field does not increase longer linearly with the current of the bump magnets.

In order to determine the deviation of the orbit from the design orbit, the electron beam was scraped on both sides of the beam pipe (each time).

Because of the excitation limits of the bump magnets in dispersion free regions, it was not possible to measure in a horizontal region without dispersion. The

horizontal measurements took place in a region with a dispersion of $0.894m$.

The used bump magnets were:
Horizontal: *WL-CH546, WL-CH522, WL-CH499*
Supporting: *WL-CH593, WL-CH569, WL-CH475, WL-CH452*
Vertical: *WL-CV652, WL-CV676, WL-CV699*
Supporting: *WL-CV605, WL-CV629, WL-CV723, WL-CV746.*

3.3 Evaluation

The measurements of the current of the bump magnets yield the bump amplitudes and with them the horizontal and vertical apertures respectively. The aperture is the distance between the center of the electron distribution and the beam pipe.

The connection between the beam lifetime and the transverse aperture is given by [8]:

- In a region with dispersion (horizontal case here):

$$\tau_{qx} = \frac{\tau_x}{\sqrt{2\pi}} \frac{e^{\frac{x^2}{2\sigma^2}}}{\frac{x^3}{\sigma^3}} \frac{1}{(1+r)\sqrt{r(1-r)}};$$
$$\sigma = \sqrt{\sigma_x^2 + \eta^2\sigma_\delta^2} \; ; \; r = \frac{\eta^2\sigma_\delta^2}{\sigma^2}.$$

  Where σ_x is the standard deviation of the horizontal beam distribution, σ_δ is the relative energy width, η is the dispersion, τ_x is the horizontal damping time and x is the horizontal aperture.

- In a region without dispersion (vertical case here):

$$\tau_{qy} = \frac{\tau_y}{2} \frac{e^{\frac{y^2}{2\sigma_y^2}}}{\frac{y^2}{\sigma_y^2}}$$

  Where σ_y is the standard deviation of the vertical beam distribution , τ_y is the vertical damping time and y is the vertical aperture.

In order to determine the transverse standard width σ_x and σ_y the plot of the measured beam lifetime as a function of the aperture is fitted. The first graph shows the lifetime as a function of the horizontal aperture without beam-beam interaction. The second graph shows the beam lifetime as a function of the vertical aperture without beam-beam interaction likewise. The last plot shows the beam lifetime as a function of the horizontal aperture with beam-beam interaction.

From the fact that the measured values follow the theoretical function, it is concluded that the transverse electron distribution is Gaussian. Note that at the HERA electron ring the beam lifetime attains a saturation value of about $10h$ because of the rest gas.

The theoretical and measured standard deviations of transverse electron distribution are given in tab. 1.

The tab. 2 gives the theoretical and measured emittances.

In the next machine studies the vertical dimension of the electron distribution should be measured with the same procedure to complete this measurements. Since

	σ_x without beam-beam interaction in m	σ_y without beam-beam interaction in m	σ_x with beam-beam interaction in m
theoretical	$1.309 \cdot 10^{-3}$		$1.303 \cdot 10^{-3}$
measured	$1.406 \cdot 10^{-3}$	$0.489 \cdot 10^{-3}$	$1.105 \cdot 10^{-3}$

Table 1: The theoretical and measured standard deviations of transverse electron distribution

	ϵ_x without beam-beam interaction in $m \cdot rad$	ϵ_y without beam-beam interaction in $m \cdot rad$	ϵ_x with beam-beam interaction in $m \cdot rad$
theoretical	$4.202 \cdot 10^{-8}$		$4.341 \cdot 10^{-8}$
measured	$4.846 \cdot 10^{-8}$	$6.331 \cdot 10^{-9}$	$3.122 \cdot 10^{-8}$

Table 2: The theoretical and measured emittances

the dispersion complicates the connection between the beam lifetime and the horizontal aperture, the measurements of the electron distribution should be repeated with a scraper in a dispersion free region, in order to get better results.

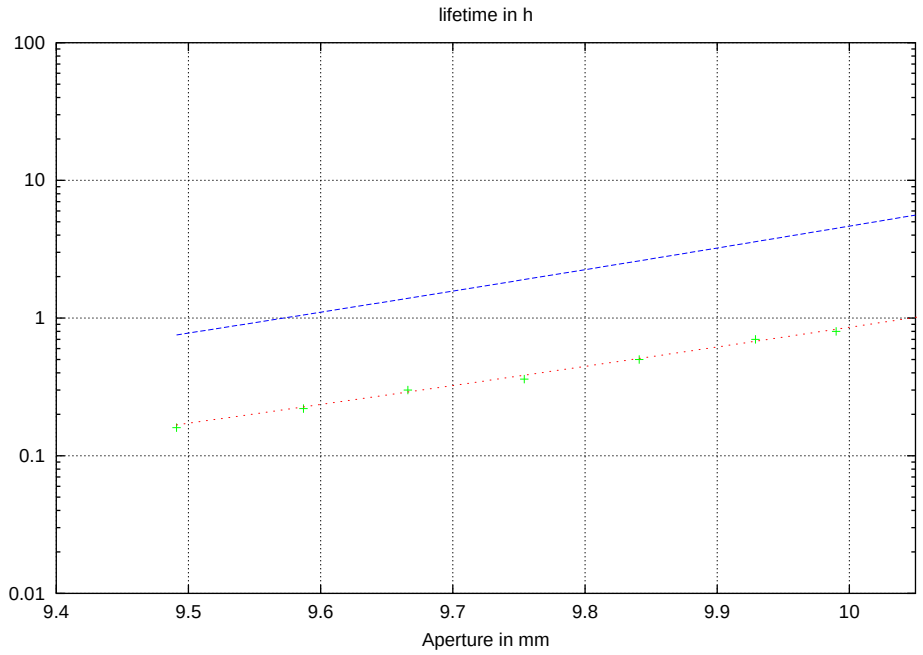

Figure 12: *Lifetime as a function of horizontal aperture without beam-beam interaction, the solid line is the theoretical function, the doted line is the fit*

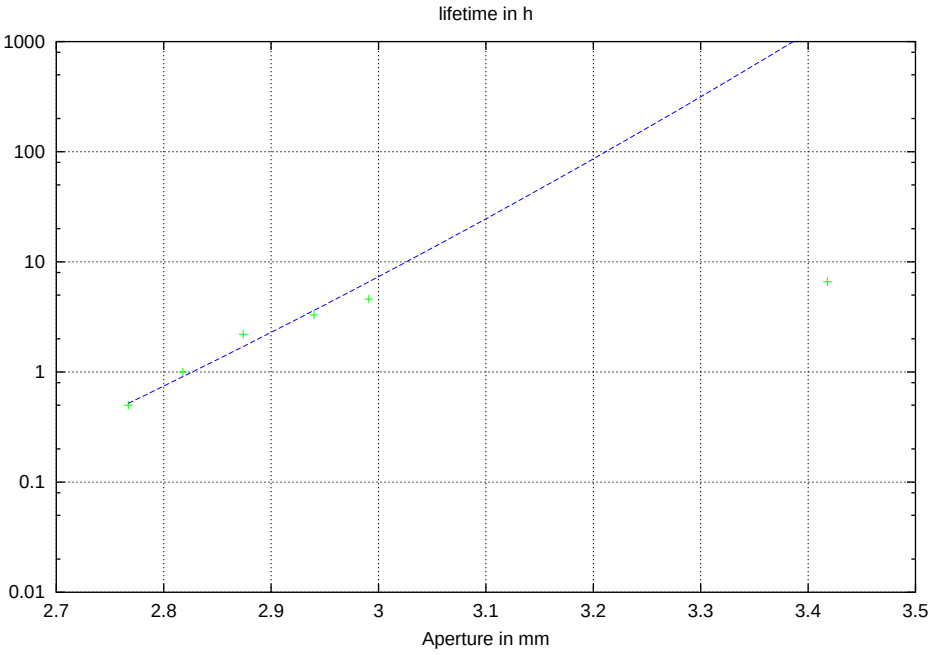

Figure 13: *Lifetime as a function of vertical aperture without beam-beam interaction, the solid line is the theoretical function.*

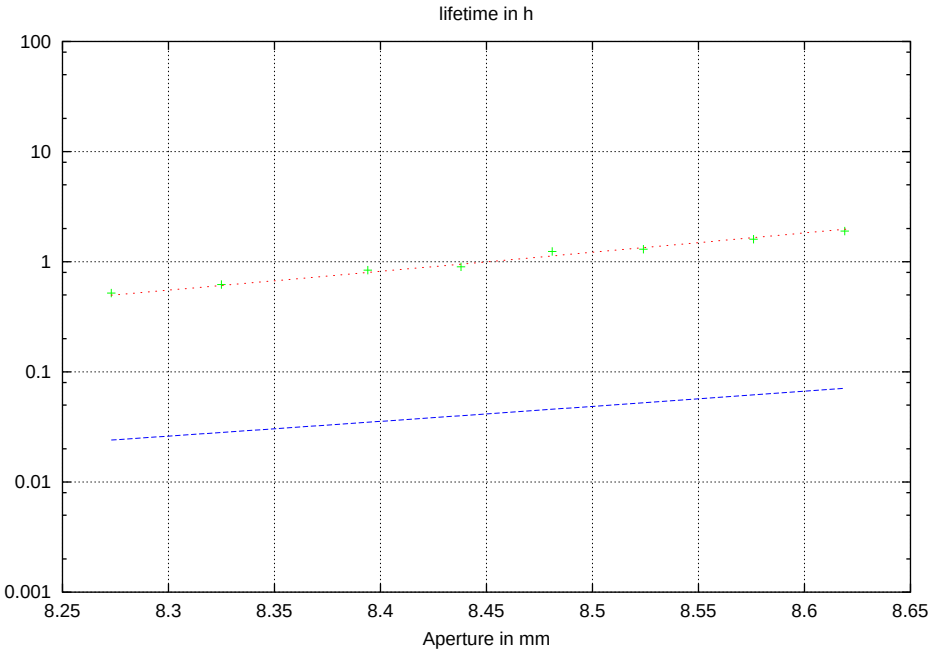

Figure 14: *Lifetime as a function of horizontal aperture with beam-beam interaction, the solid line is the theoretical function, the doted line is the fit*

4 The Emittance in HERA-e for Different RF Frequencies

Date: 1998, Dec. 16, 11am–9pm, Logbook XXXIV, page 153–157
Date: 1998, Dec. 20, 6pm–11pm, Logbook XXXIV, page 201–202

In the HERA luminosity upgrade the horizontal emittance of the electron beam has to be reduced from currently 41πnm to approximately 22πnm [5]. Here the current emittance is computed by assuming that the closed orbit goes through the center of the quadrupoles, which is only the case for a central RF frequency f_c. This emittance reduction can be obtained either by stronger focusing or by an RF frequency shift, which leads to a closed orbit deviation in Quadrupoles and thus changes the damping partition numbers [1]. In order to test whether the latter method of reducing the emittance works as expected, the RF frequency was shifted in the current HERA-e ring and the emittance was measured by three different means: by the synchrotron light monitor and by the luminosity monitors of H1 and Zeus.

4.1 Introduction

The transverse emittance ε_x and the squared relative energy deviation σ_δ of an electron storage ring are given by [4]

$$\varepsilon_x = \frac{C_q\gamma^2}{1-\mathcal{D}}\frac{<|G|^3\mathcal{H}>_s}{<G^2>_s}\ , \quad \sigma_\delta^2 = \frac{C_q\gamma^2}{2+\mathcal{D}}\frac{<|G|^3>_s}{<G^2>_s}\ , \tag{2}$$

$$\mathcal{D} = \frac{<\eta G(G^2+2K)>_s}{<G^2>_s}\ , \quad \mathcal{H} = \frac{1}{\beta}[\eta^2+(\beta\eta'+\alpha\eta)^2]\ , \tag{3}$$

with the curvature $G(s)$ of and the focusing strength $K(s)$ on the closed orbit, which is parameterized by its arc length s. The parentheses $<\ldots>_s$ indicate an average around the ring and $\eta(s)$ is the periodic dispersion. The optic functions $\alpha(s)$ and $\beta(s)$ are used and $C_q \approx 384$fm is a constant. On the design orbit of a separated function ring, which HERA-e is to a good approximation, $G(s)\cdot K(s) = 0$ around the ring. The dependence of the denominator on an RF frequency shift is investigated in section 6.1. Also the numerator changes somewhat when the energy is changed by a shifted frequency. The dispersion η changes as well as β and α when the closed orbit goes off axis through quadrupoles and sextupoles. The calculations which are subsequently compared to measurements have been obtained with these effects taken into account. The horizontal emittance has been measured in the following different ways:

The synchrotron light monitor images synchrotron light coming out of a dipole magnet onto a CCD video camera. Since the light optics is point to point imaging, a profile of the beam spot is produced; electrons with different slopes

emit photons which illuminate the same CCD pixel. Relative to the horizontal beam size σ_h, the synchrotron light spot is too big due to diffraction and other problems of the light optics as discussed in section 5. This error ξ is subtracted quadratically from the synchrotron light spot σ_s. The emittance is thus obtained from the synchrotron light spot by

$$\varepsilon_x = (\sigma_s^2 - (\eta\sigma_\delta)^2 - \xi^2)\frac{1}{\beta} \; . \tag{4}$$

Also the energy contribution $\eta\sigma_\delta$ due to a dispersion at the synchrotron light monitor has to be subtracted, where we used calculated rather than measured values for η, σ_δ, and β. The calculated beta function describes reality quite well, which has been verified by shifting the synchrotron light spot with closed orbit bumps. The error ξ appears to be not well known and the emittance obtained from the synchrotron light spot might be wrong by a constant offset. By comparing the measured emittance as a function of RF frequency shift Δf with the corresponding computed function $\varepsilon_x(\Delta f)$, we determined this offset as well as a deviation Δf_0 between the current operation RF frequency f_0 and the central RF frequency f_c.

The luminosity monitors from H1 and ZEUS measure the bremsstrahlung produced by electrons scattering of particles in the interaction region. Since no proton been was stored during the measurements presented here, the electrons scattered off rest gas particles only. The bremsstrahlung is radiated in a cone with angle ϑ which depends on the scattering particle and is approximately $\frac{1}{\gamma}$. At ZEUS this radiation is detected $L = 107.6$m downstream by a detector with resolution $r = 1.5mm$, where the rms photon spot size σ_{ph} is related to the electron emittance by

$$\varepsilon_x = \beta^\star \frac{\sigma_{ph}^2 - (\eta^\star + L\eta'^\star)^2\sigma_\delta^2 - r^2 - (L\vartheta)^2}{L^2 + (\beta^\star - \alpha^\star L)^2} \tag{5}$$

where $\star$ indicates calculated values at the interaction point. Similar values apply for the H1 luminosity monitor. In evaluating these measurements from H1 and Zeus the change of $\beta^\star$, $\alpha^\star$, and $\eta^\star$ with the RF frequency were all taken into account.

4.2 The Measurement

In order to analyze the feasibility of emittance reduction by stronger focusing in the FODO cells, a 72° optics has been computed and installed in HERA-e as described in section 2. In this optics the dispersion at the synchrotron light monitor is very small and the synchrotron spot size σ_s is therefore hardly influenced by the energy width σ_δ of the beam. For this optics, figure 15 shows the rms beam size $\sigma_h = \sqrt{\sigma_s^2 - \xi^2}$ of the electron beam as a function of RF frequency shift Δf away from the current operation frequency. An error $\xi = 0.769$mm of the synchrotron monitor has been subtracted quadratically from the synchrotron spot size σ_s in order to match the curve's vertical position to the computed $\sigma_h(\Delta f)$, which is also shown in this figure. This error of the monitor can be estimated as described in section 5 to be 0.579mm, which does not seem to be very far away from the fitted value considering the difficulty of the estimation.

In the simulation the current operation frequency f_0 has been assumed to be 175Hz lower than the central frequency f_c, in order to match the curve's horizontal

position to the measured data. Simulation and measurement match quite well for this setting of ξ and Δf_0. The same measurement and calculation was performed

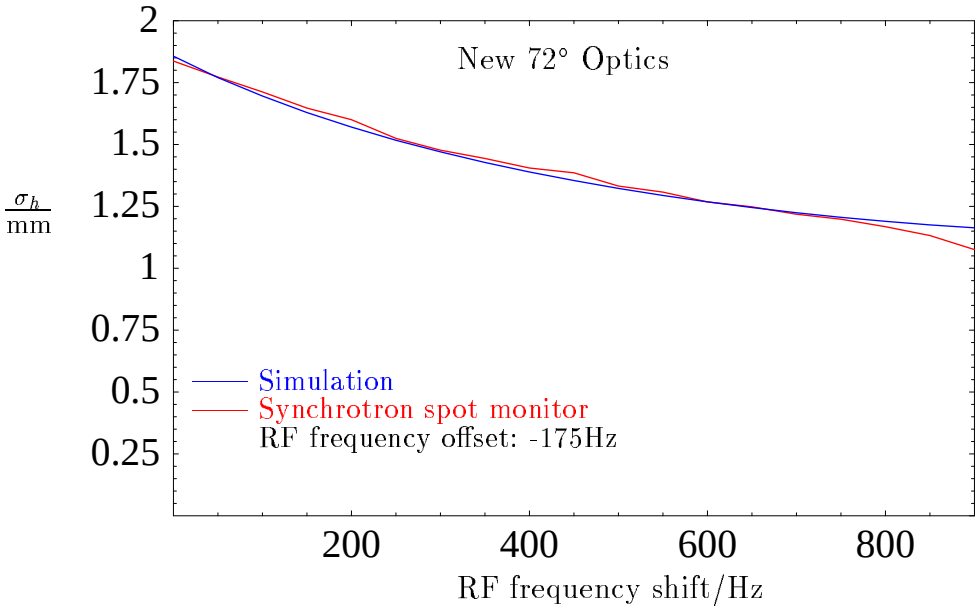

Figure 15: Horizontal beam size σ_h at the synchrotron light monitor in the new 72° optics as a function of a shift in RF frequency: Computed with MAD [2] and measured with the synchrotron light monitor.

for the current 60° luminosity optics of HERA-e. There the dispersion is 0.86m at the synchrotron light monitor. A change in horizontal beam size $\sigma_h = \sqrt{\beta\epsilon_x + \eta^2\sigma_\delta^2}$ with RF frequency shift is hardly observed since the reduction of ϵ_x is compensated by an increase in the energy spread σ_δ. Figure 16 shows the rms beam size σ_h at the synchrotron monitor as a function of RF frequency shift. The error ξ and the Frequency offset $\Delta f_0 = f_0 - f_c$ between operation frequency and central frequency were also taken to be 0.769mm and -175Hz, respectively. This seems reasonable since neither the error of the synchrotron light monitor, nor the length of the closed orbit which goes through the center of the quadrupoles and defines the central frequency f_c, depend on the focusing strength in the ring.

Figure 17 and 18 show the computed emittance and the emittance obtained from the synchrotron monitor with $\xi = 0.769$mm and $\Delta f_0 = -175$Hz by equation 4. Considering the problematic data in the 60° case due to a large dispersion at the synchrotron monitor, the agreement between measurement and simulation appears to be satisfactory.

The emittances obtained from the luminosity monitors of H1 and Zeus, however, are hardly acceptable. As shown in figure 17 and 18, these values for the emittance hardly vary with RF frequency and are both rather low even without RF frequency shift. Furthermore, not even a reduction in emittance by stronger focusing in the FODO cells can be observed with the luminosity measurements. These measurements are not understood so far.

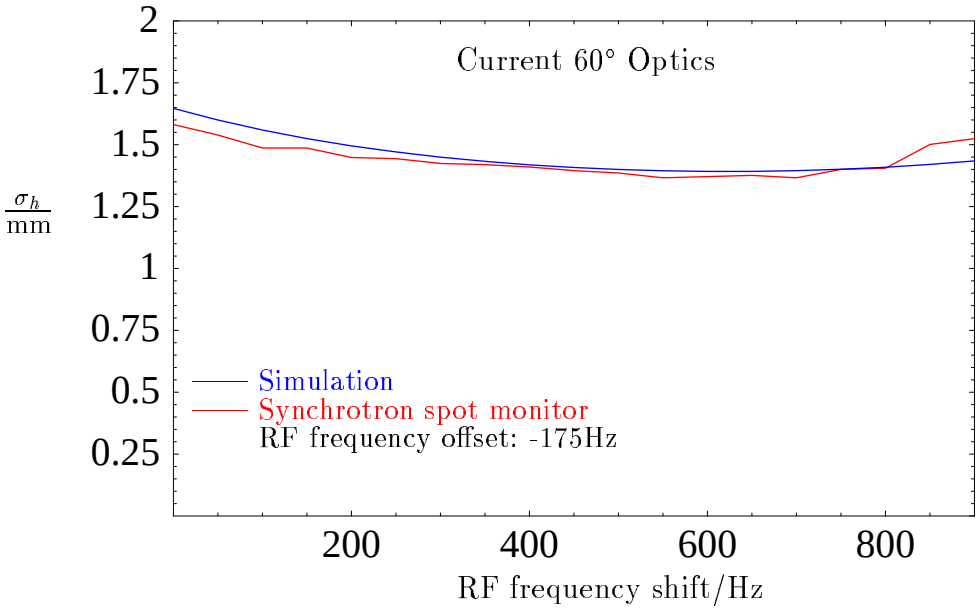

Figure 16: Horizontal beam size σ_h at the synchrotron monitor as a function of RF frequency shift for the current 60° optics: Computed with MAD [2] and measured with the synchrotron light monitor.

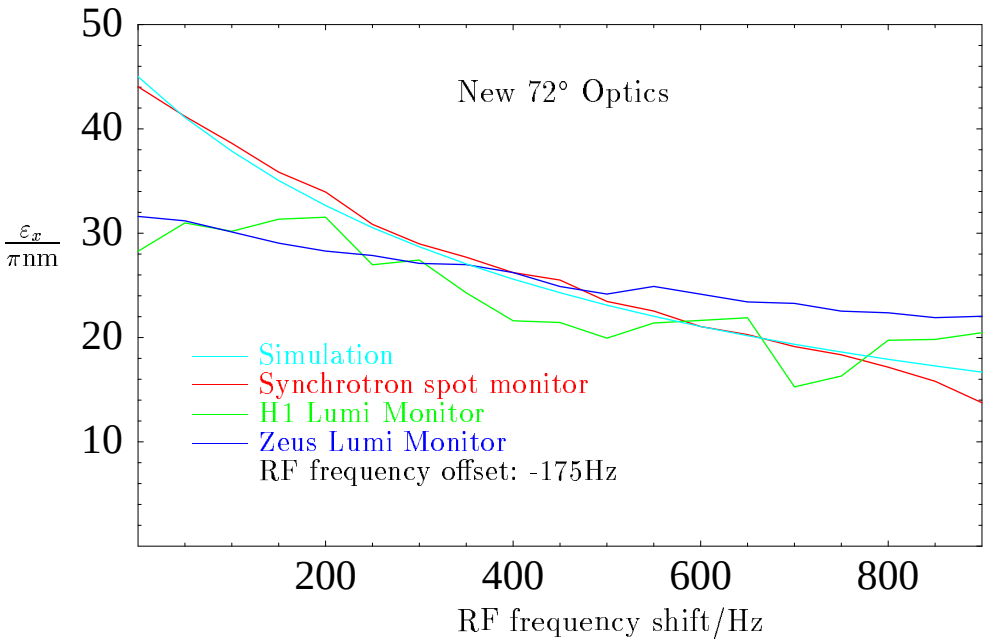

Figure 17: The simulated emittance reduction with an increased RF frequency is compared to the emittance deduced from the H1 and Zeus luminosity monitors for the new 72° optics and with the emittance measured by the synchrotron light monitor.

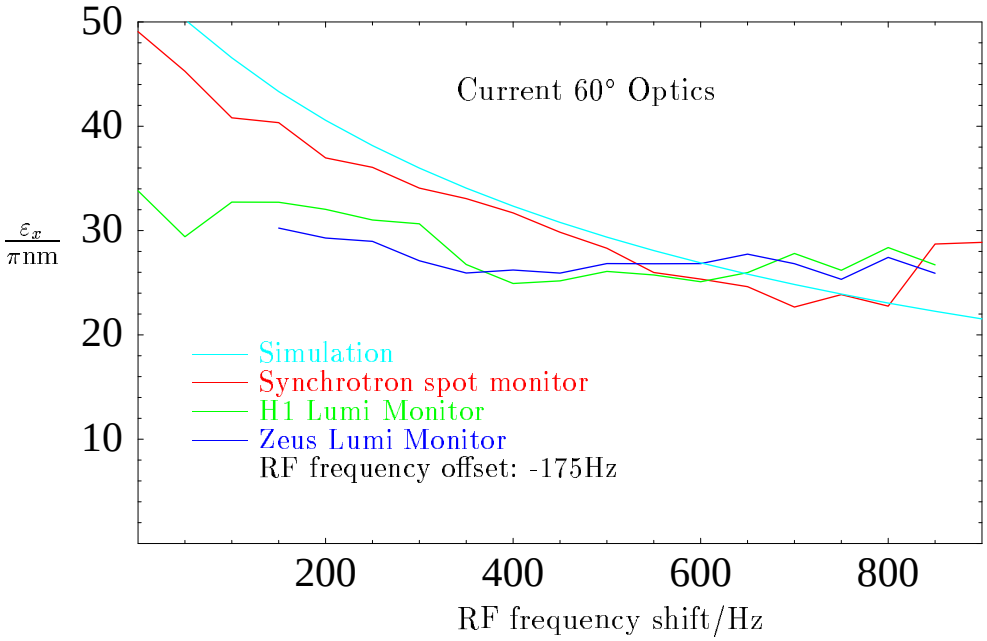

Figure 18: The simulated emittance reduction with an increased RF frequency is compared to the emittance deduced from the H1 and Zeus luminosity monitors for the current 60° optics and with the emittance measured by the synchrotron light monitor.

4.3 Conclusion

The synchrotron light monitor indicates that the reduction of horizontal electron emittance with an RF frequency shift follows theoretical predictions and can thus be used in the luminosity upgrade project. Besides the reduction of the horizontal emittance with an increase of the RF frequency, also the reduction of the emittance by increasing the focusing per FODO cell from 60° to 72° could be observed and can thus be used in the luminosity upgrade project. Since the emittances obtained by both luminosity monitors do not reflect this apparently successful emittance reduction, it seems advisable to perform an independent measurement of the emittance reduction with a wire scanner as soon as it is installed in HERA-e.

5 Gauging the HERA-e SR Monitor

Date: Dec. 16, 1998, 7am to 3pm Logbook XXXIV, page 143–144

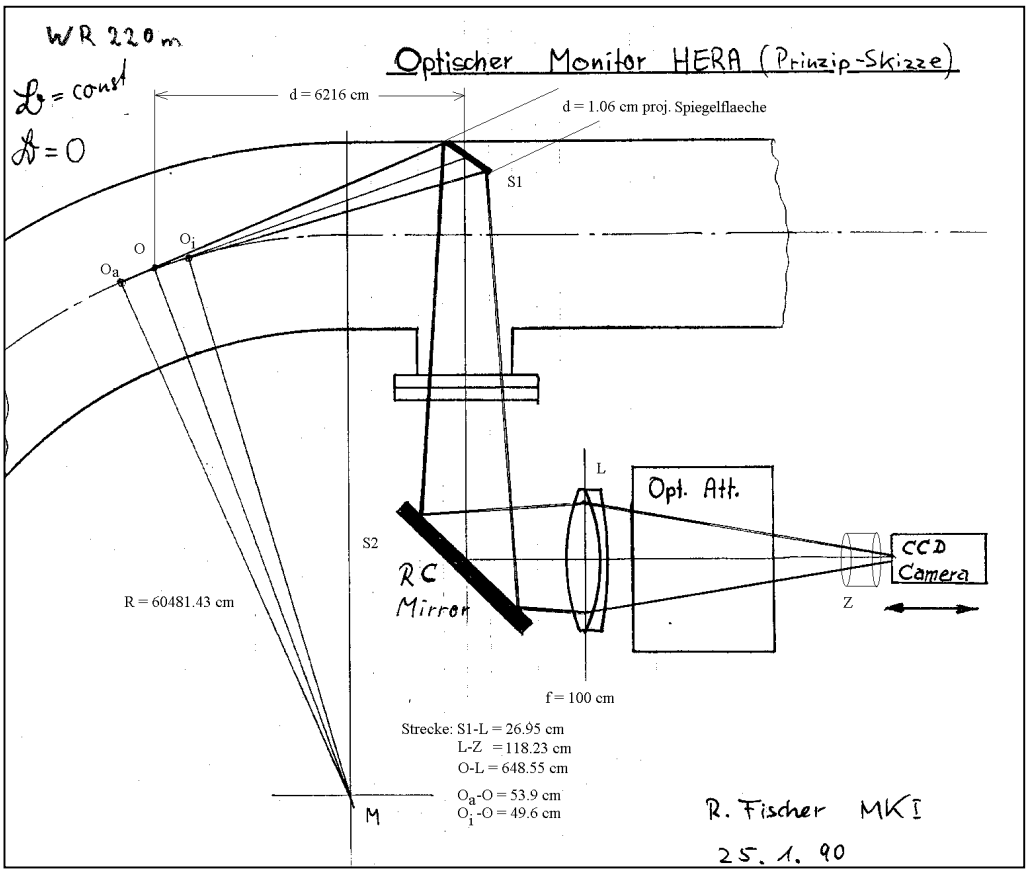

Abb. 1 Synchrotronlicht Monitor in HERAe

Die Geometrische Abmessungen des Elektronenstrahls wird u.a. durch seine Emittanzen bestimmt. Der von der Kamera gemessene Lichtfleck der Synchrotronstrahlung muß in seinen Abmessungen auf den Ursprungsort O zurückgerechnet werden um Aussagen über die Dimensionen und Emittanzen des Strahles machen zu können. Dazu wurden die folgenden Eichungen durchgeführt:
A) Eichung durch Kamera (Lichtoptische Parameter als bekannt vorausgesetzt)
B) Eichung mit Gitter (Lichtoptische Parameter müssen teilweise bekannt sein)
C) Eichung mit Strahl (Überprüfung der Parameter)

A) Eichung durch Kamera
Aus den Experimenten am 12.5.98, Notizen ist bekannt, daß der CCD Chip der Kamera eine lichtempfindliche Dimension in horizontaler Richtung von H=8.38 mm hat. Nach CCIR Norm wird ein Verhältnis von H:B = 2:3 in einem Bildspeicher (hier Frame Grabber) abgespeichert. Damit ergibt sich für die vertikale Richtung eine Dimension von V=5.59 mm lichtempfindliche Fläche. Mit dem Vergrößerungsfaktor der Lichtoptik von 1.85 ergibt sich damit, daß die Kamera eine Fläche von

H:V = 8.38mm * 1.85 : 5.59mm * 1.85 = 15.5mm : 10.34mm
beobachtet. Diese Werte wurden Anfangs zur Bestimmung der Lichtfleckdimension des Synchrotronlichtes herangezogen. Eine genauere Eichung ist mit B) möglich.

B) Eichung mit Gitter
Vor der Videokamera befindet sich ein Objektiv zur Nachvergrößerung des virtuellen Zwischenbildes des SR-Lichtes. An dieser Stelle wurde ein Strichmuster mit 0.1 mm Abstand eingebracht und aufgenommen

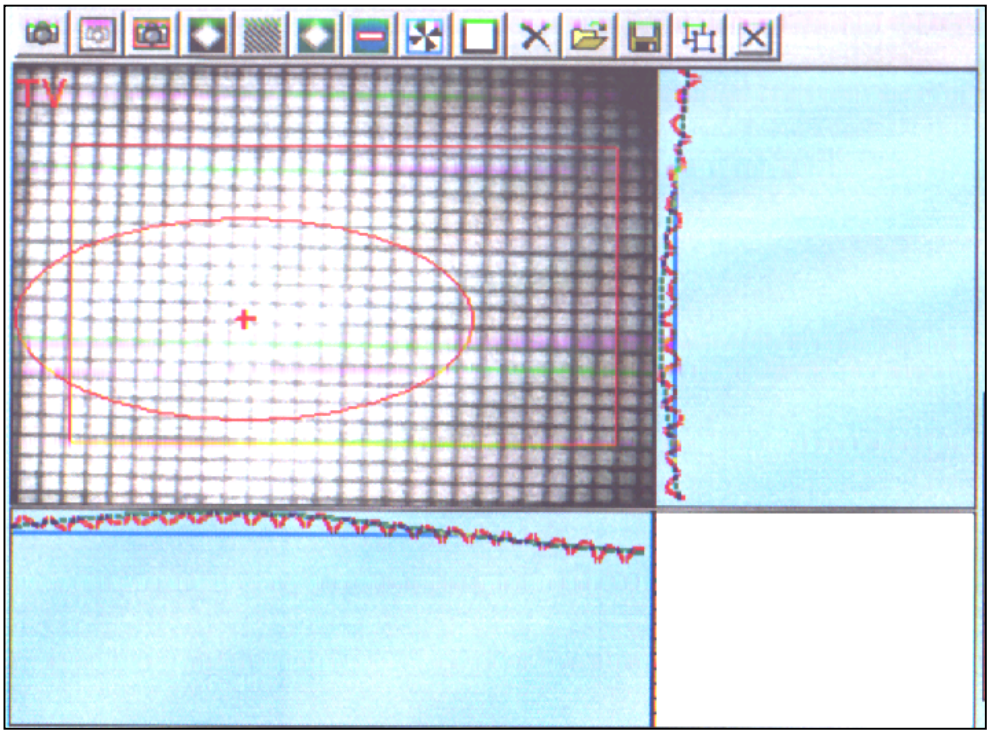

Abb. 2.: Aufgenommenes Strichmuster

Horizontal wurden H=2.76 mm beobachtet, vertikal waren es V=2.26 mm. Anhand des Musters kann die am Ursprungsort beobachtbare Fläche errechnet werden: Der Vergrößerungsfaktor vom virtuellen Zwischenbild zum Ursprungsort ist G/B = 5.485. Damit ergibt sich für den Ursprung:
H : V = 2.76 mm * 5.485 : 2.25 * 5.485 = 15.14 mm : 12.34 mm
Das stimmt im Rahmen der Messungen horizontal gut mit A) überein, vertikal scheint jedoch die Annahme über die Chipgröße oder das Abspeicherverhältnis etwas daneben zu liegen. Dieses neue Maß wird ab sofort in der Auswertung des SR-Bildes als Eichung eingesetzt.

C) Eichung mit Strahl
Die durch Messung B) gewonnene Eichung wurde am 15.12.98 mit dem Strahl überprüft. Im Bereich des Ursprungs wurde der Strahl mit einer abgeschlossenen Beule definiert abgelenkt. Anhand der Korrekturspulen-Parameter und der Strahloptik-Parameter wurde die Strahlposition im Ursprung genau errechnet. Dank an Eliana, von der auch die folgenden Abbildungen stammen.

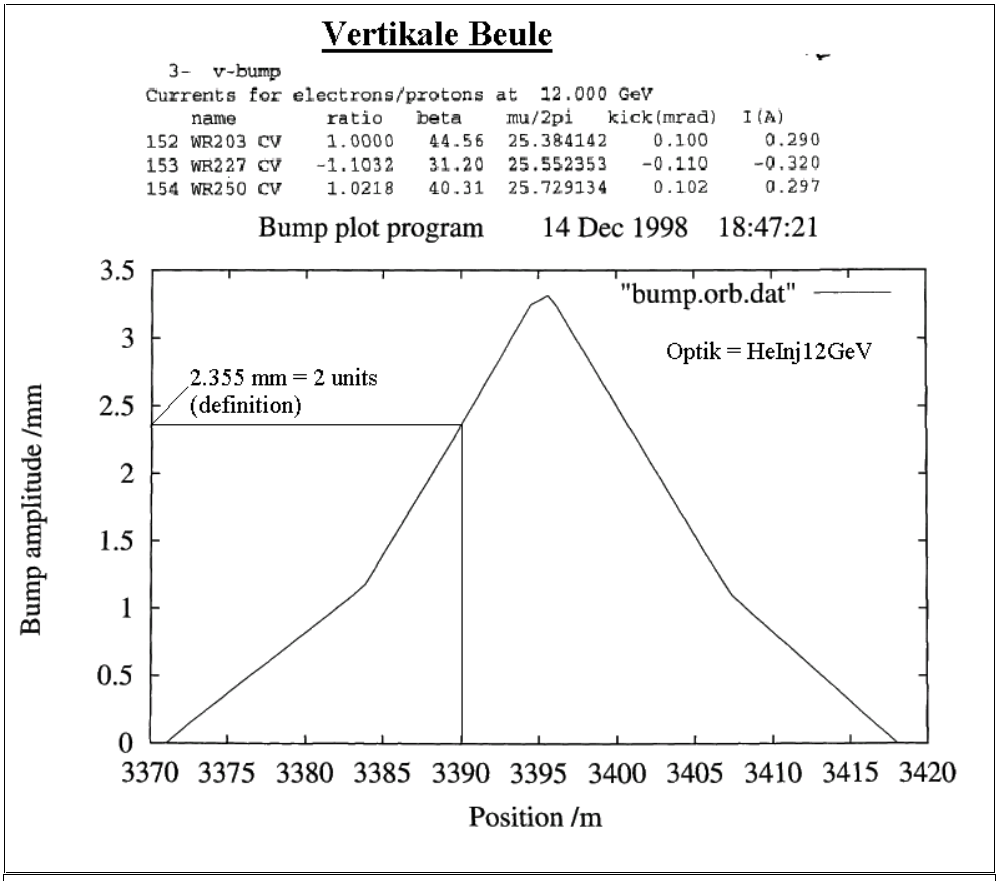
Vertikale Beule
3- v-bump
Currents for electrons/protons at 12.000 GeV
name ratio beta mu/2pi kick(mrad) I(A)
152 WR203 CV 1.0000 44.56 25.384142 0.100 0.290
153 WR227 CV -1.1032 31.20 25.552353 -0.110 -0.320
154 WR250 CV 1.0218 40.31 25.729134 0.102 0.297
Bump plot program 14 Dec 1998 18:47:21
"bump.orb.dat"
Optik = HeInj12GeV
2.355 mm = 2 units
(definition)
Bump amplitude /mm
Position /m

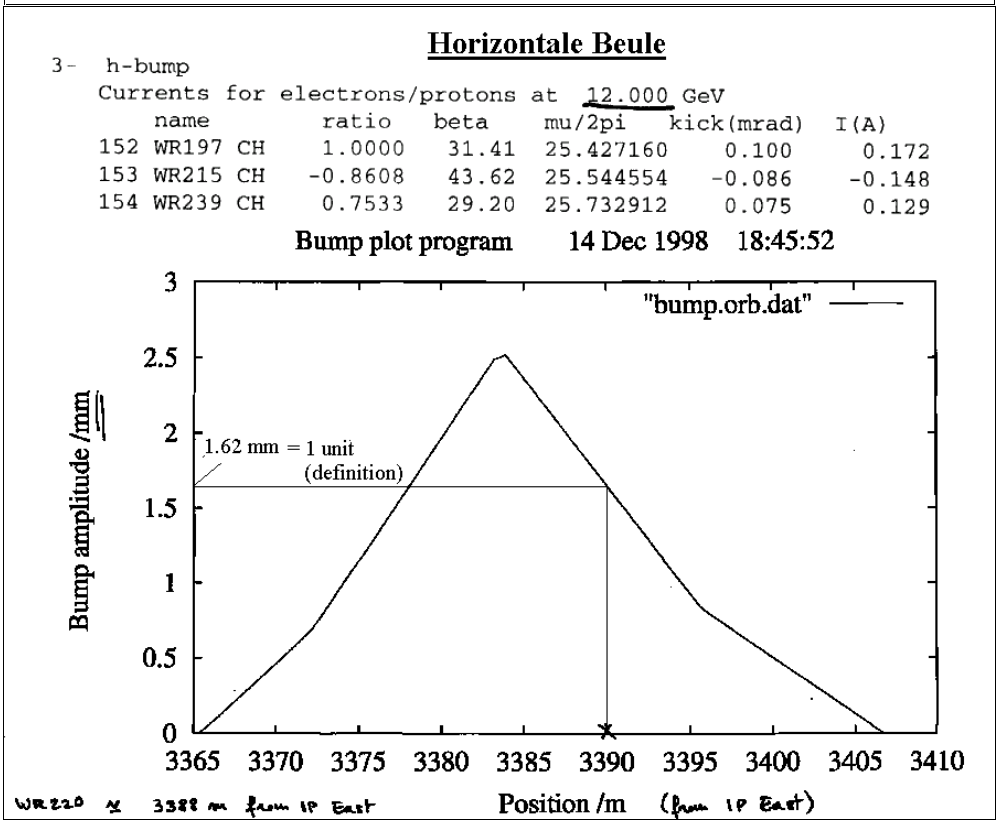
Horizontale Beule
3- h-bump
Currents for electrons/protons at 12.000 GeV
name ratio beta mu/2pi kick(mrad) I(A)
152 WR197 CH 1.0000 31.41 25.427160 0.100 0.172
153 WR215 CH -0.8608 43.62 25.544554 -0.086 -0.148
154 WR239 CH 0.7533 29.20 25.732912 0.075 0.129
Bump plot program 14 Dec 1998 18:45:52
"bump.orb.dat"
1.62 mm = 1 unit
(definition)
Bump amplitude /mm
WR220 x 3388 m from IP East
Position /m (from IP East)

Abb. 3

Die in der Abbildung gezeigten (additiven) Ströme in den Korrekturspulen erzeugen eine Ablage des Strahles im Ursprung des SR-Lichtes von 1.62 mm (horizontal) und 2.355 mm (vertikal). Diese Ströme werden im folgenden mit 1 Unit (horizontal) bzw. 2 Units (vertikal) definiert. Diese Beulen wurden über mehrere Units eingestellt und die vom Monitor gemessene Ablage mit der theoretischen Ablage verglichen. Die Messungen wurden bei 12 GeV und bei 27.5 GeV durchgeführt, wobei sich die Spulenströme linear mit der Energie skalieren. Es war immer die Injektionsoptik eingestellt. Die Abbildung 4 zeigt ein Beispiel der Messung bei 12 GeV, horizontal.

Die Tabelle zeigt die Meßergebnisse:

Beule	Horizontal		Vertikal	
	12 GeV	27.5 GeV	12 GeV	27.5 GeV
Units	Differenz der gem. Ablage zur vorherigen Beule (Unit) [mm]			
-2	1.58			
-1	1.38	1.5	0.79 0.62	0.9
0	1.61	1.43	1.26 1.13	1.21
1	1.77	1.66	1.27 1.1	0.94
2	1.83	1.7	0.75 0.81	0.93
3			0.85	1.29
Mittelwert	1.63	1.57	1.19	1.05
Erwartet	1.62	1.62	1.18	1.18

Die Übereinstimmung bei 12 GeV ist sehr gut, die leichten Abweichungen bei 27.5 GeV sind möglicherweise durch eine Abweichung in der Betafunktion zu erklären.
Bei den vertikalen Messungen wurde beobachtet, daß des einen Bereich gibt, in dem die Ablage proportional zur Beule ist, außerhalb dieses Bereiches wurden Reflexionen und Absorbtion des Lichtes beobachtet[1]. Dieses verfälscht sowohl die Positions- als auch die Emittanzmessung. Zur Überprüfung der Eichung wurde nur der lineare Bereich herangezogen.

Zusammenfassung

Die Eichung des Monitors aus B) stimmt

Dank an Fedor für die Unterstützung während der Meßschicht

[1] Die Beule ändert auch den Winkel des SR-Lichtes. Das Licht trifft dann bei ungeeigneter Beule unter flachen Winkel auf das Strahlrohr und wird reflektiert. Solche Bedingungen waren bei der Default-Einstellung gegeben (File). Bei zukünftigen Messungen muß immer auf eine saubere Lichtellipse geachtet werden!

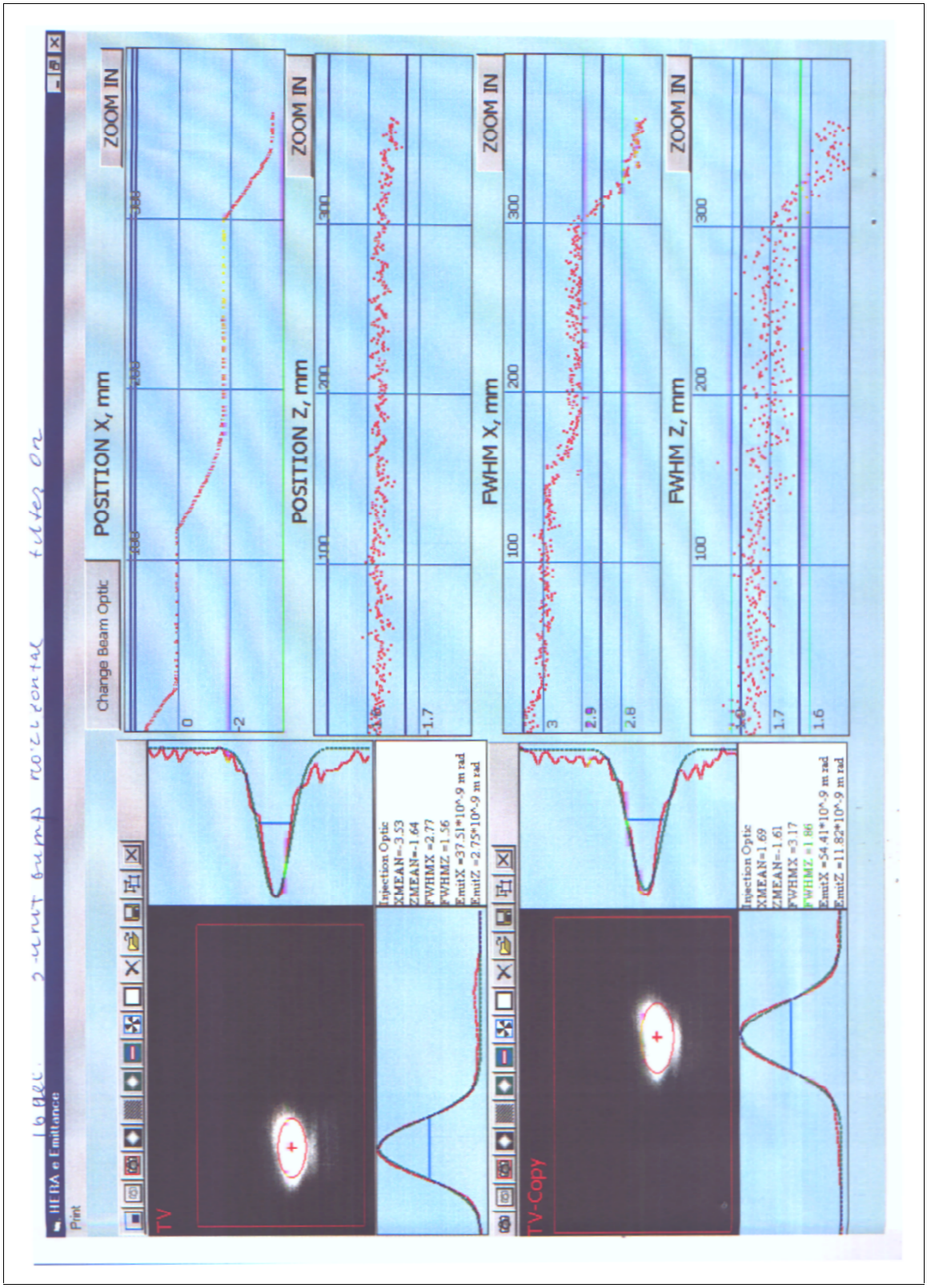
Print
Change Beam Optic
POSITION X, mm
ZOOM IN
POSITION Z, mm
ZOOM IN
FWHM X, mm
ZOOM IN
FWHM Z, mm
ZOOM IN
TV
TV-Copy
Injection Optic
XMEAN=-3.53
ZMEAN=-1.64
FWHMX =2.77
FWHMZ =1.56
EmitX =37.51*10^-9 m rad
EmitZ =2.75*10^-9 m rad
Injection Optic
XMEAN=1.69
ZMEAN=-1.61
FWHMX =3.17
FWHMZ =1.86
EmitX =54.41*10^-9 m rad
EmitZ =11.82*10^-9 m rad

Abb.4

Anhang 1: Zur Auflösungsgrenze des SR-Monitors

Die klassische Berechnung der Auflösungsgrenze eines SR-Monitors ist in diversen Referenzen beschrieben (Ref. 1) Im Folgenden werden die Abweichungen von dieser Betrachtungsweise diskutiert:

1) Beugung:
Die klassische Beugung behandelt die Beugungserscheinung an einer scharfen Kante. Das SR Licht hat jedoch vertikal keine scharfe Kante sondern ist mehr oder weniger gaussförmig. Daher gilt die klassische Beugungsformel nicht mehr exakt. Ref. A1 behandelt dieses Problem und kommt zu dem Schluß, daß zwei Punkte zur Beugung beitragen:
a) Der Abstrahlwinkel Ψ ist größer in Realität als in der Gauss Näherung (0.79 $\rightarrow$ 1.08 mrad bei Tristan, siehe Fig. unten)
b) Das 1. Beugungsmaximum liegt bei einem gaussförmigen Strahl bei $\sigma_{Beug} = 1/\pi * \lambda/\Psi$
Mit den HERA Parametern ergibt sich dann:
$\sigma_{Beug} \approx 218$ µm ($\Psi = 0.8$ mrad, $\lambda = 550$ nm) vertikal

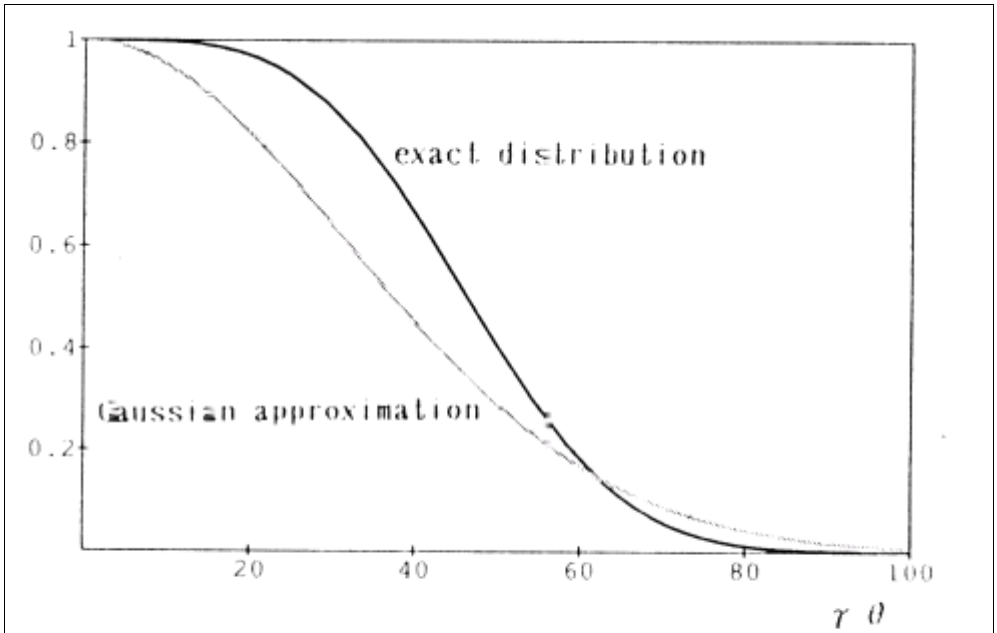

Fig. 1 Angular distribution of the 500 nm component of the synchrotron radiation from the TRISTAN MR bending magnet (246 m bending radius) operated at 30 GeV, and its Gaussian approx mation.

Abb. A1

In der horizontalen Ebene tragen die scharfen Kanten des Spiegels zur Beugung bei und das 1. Beugungsmaximum ist daher klassisch zu berechnen:
$\sigma_{Beug} = 0.61 * \lambda/\theta/2$ (horizontal) = 395 µm

mit Winkelakzeptanz (horizontal): $\theta/2 = 0.85$ mrad (definiert durch die Spiegeldimensionen) und $\lambda = 550$ nm

2) Tiefenschärfe

Die in der Literatur angegebene Formel für die Tiefenschärfe bezeichnet den maximalen Radius eines Lichtfleckes, der durch den Effekt der Tiefenschärfe zustande kommt, das liefert jedoch keine Aussage über die Verteilung des Lichtes.

Annahme: Auf der Beobachtungsstrecke (l = 1035 mm in HERAe) wird das Licht in einen Winkelbereich zwischen 0 und 0.8 mrad homogen abgestrahlt. Der Fokus der Optik liegt in der Mitte der Beobachtungsstrecke. Durch die Tiefenschärfe ergibt sich auf der Bildebene die Verteilung aus Fig. A2 (Abbildungsmaßstab 1:1).

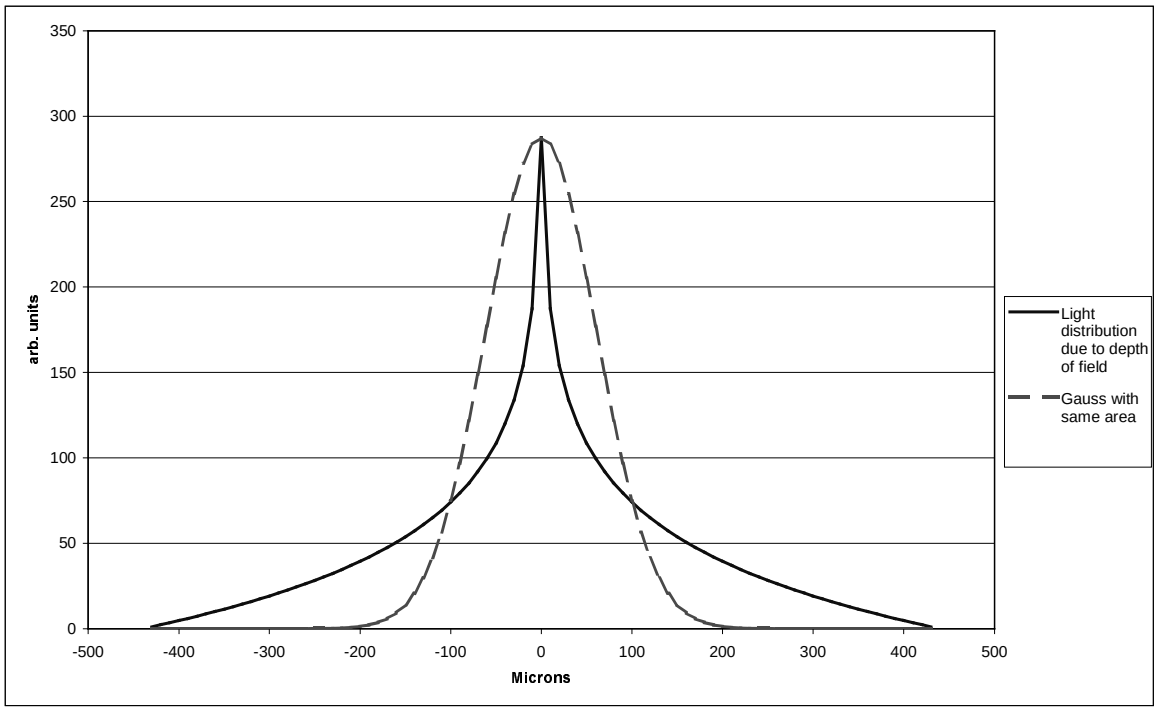

Fig. A2

Die Maximale Ausdehnung (Radius) der Verteilung wird durch die Formel $R_{tief} = L/2 * \theta/2 = 440$ μm beschrieben. Die Auflösung eines Bildes ist jedoch deutlich besser bei einer solchen Verteilung. Eine (zugegebener Maßen sehr ungenaue) Näherung wird durch eine Gausskurve beschrieben, die den gleichen Flächeninhalt wie die Lichtverteilung hat (siehe Fig. A1). Damit ergibt sich für $\sigma_{tief} = 61$ μm.

Konsequenzen:

Die gesamte Auflösung des SR Monitors berechnet sich dann neu wie folgt:

mit: $\sigma_{kamera} = 37$ μm; $\sigma_{kurve} = \rho\, \theta^2/8 = 219$ μm (aus Ref 3):

vertikal:

$\sigma_{korr} = (\sigma_{Beug}^2 + \sigma_{tief}^2 + \sigma_{kamera}^2)^{1/2} = \underline{229\ \mu m}$

horizontal:

$\sigma_{korr} = (\sigma_{Beug}{}^2 + \sigma_{tief}{}^2 + \sigma_{kurve}{}^2 + \sigma_{kamera}{}^2)^{1/2} = \underline{457\ \mu m}$

Die Tiefenschärfe führt dazu, daß bei der vertikale Lichtverteilung die Schwänze der Verteilung aus der Tiefenschärfe sichtbar über einem Gaussfit liegen sollten. Die Beispiele aus Abb. 4 und Abb. A3 zeigen dies deutlich. Solche Verteilungen sind ständig am Monitor zu beobachten. Diese Schwänze sollten bei einem Fit des Profils nicht mit beitragen.

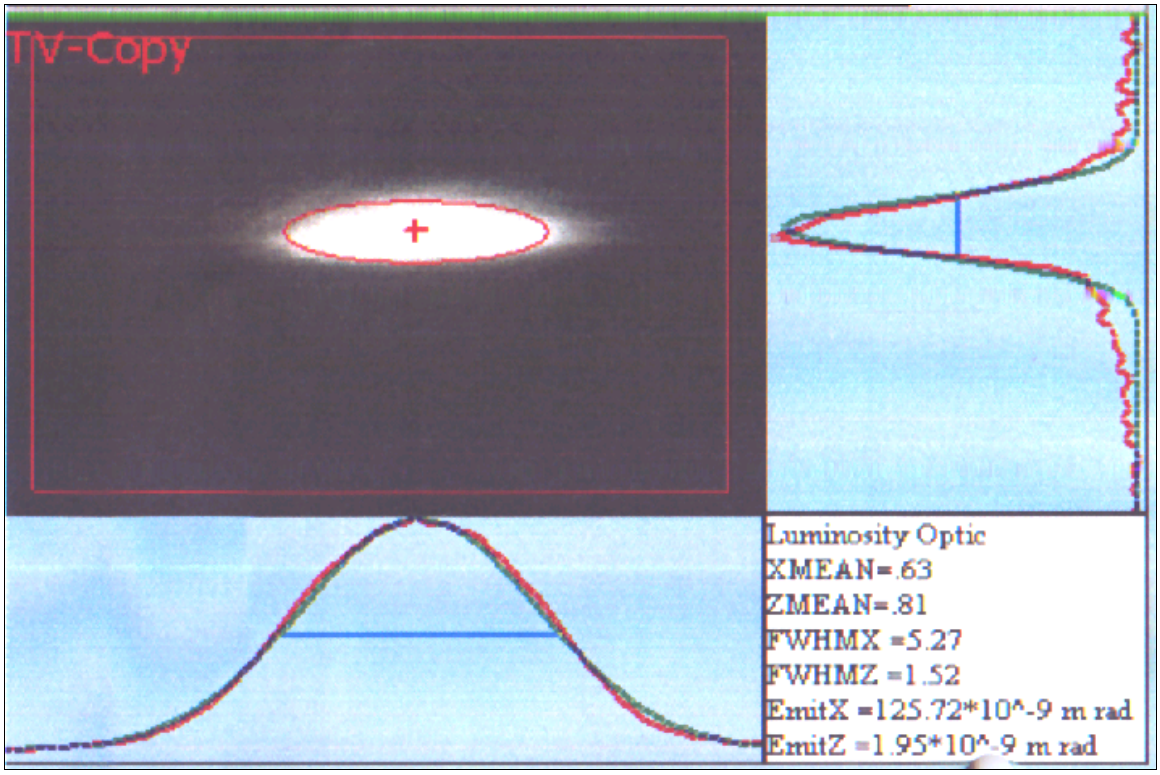

Fig. A3

Ref. 1: **OPTICAL RESOLUTION OF BEAM CROSS-SECTION MEASUREMENTS BY MEANS OF SYNCHROTRON RADIATION.** By A. Hofmann, F. Meot (CERN). CERN/ISR-TH/82-04, Feb 1982. 28pp. Published in Nucl.Instrum.Meth.203:483,1982).

Ref. 2: **ON OPTICAL RESOLUTION OF BEAM SIZE MEASUREMENTS BY MEANS OF SYNCHROTRON RADIATION**. By A. Ogata (KEK, Tsukuba). 1991. Published in Nucl.Instrum.Meth.A301:596-598,1991

Ref. 3: **Synchrotronstrahlungs-Profilmonitor in HERA e**; K. Wittenburg, R. Fischer, -MKI-, Internal Note Witt98-01, 5.6.1998)

6 The Central Frequency of HERA-e

As described in section 4, the horizontal electron emittance in HERA has to be reduced in the luminosity upgrade project. The methods of choice are stronger focusing in the arcs and increasing the RF frequency. There is a leverage for decreasing the emittance by the latter method only if the current operation RF frequency f_0 is not too far above its central value f_c. Several experiments were therefore performed during the December 1998 machine studies to specify a possible shift of the current RF frequency away from f_c.

The current frequency f_0 of the RF system is known very accurately. The central frequency f_c, however, is defined by the length of the specific closed orbit which goes through the center of quadrupoles; and five methods were applied to measure this frequency. In section 4 a deviation of f_0 from f_c was derived from the emittance reduction produced by RF frequency shifts in the current 60° and the new 72° optics. Four other methods are described in the subsequent subsections. The results together with an estimate of the random errors of these methods are shown in the following table. They all show that the current frequency f_0 is not severely above f_c; more likely f_0 is even below f_c. The frequency can therefore safely be increased to reduce the horizontal emittance in the luminosity upgrade project.

Measurement	$\Delta f_0 = f_0 - f_c$	random error
Beam loss at damping poles	-163 Hz	± 20 Hz
Extrapolation of damping times	-250 Hz	± 150 Hz
Horizontal center of sextupoles	+130 Hz	± 25 Hz
Vertical center of sextupoles	-70 Hz	± 50 Hz
Emittance change with frequency	-175 Hz	± 70 Hz

6.1 The Central Frequency Determined from the Damping Poles

Date: 1998, Dec. 19, 4pm, Logbook XXXIV, page 186
1998, Dec. 19, 7pm, Logbook XXXIV, page 188
1998, Dec. 20, 9pm, Logbook XXXIV, page 202
1999, Jan. 9, 6am, Logbook XXXIV, page 230
1999, Mar. 13, 7pm, Logbook XXXVI, page 67

The transverse and longitudinal emittances ε_x and ε_s of an electron storage ring are inversely proportional to the damping partition numbers $J_x = 1 - \mathcal{D}$ and $J_s = 2 + \mathcal{D}$ [4],

$$\varepsilon_x \propto \frac{1}{1-\mathcal{D}} \ , \quad \varepsilon_s \propto \frac{1}{2+\mathcal{D}} \ , \quad \mathcal{D} = \frac{< \eta G(G^2 + 2K) >_s}{< G^2 >_s} \ , \tag{6}$$

with the curvature $G(s)$ of and the focusing strength $K(s)$ on the closed orbit, which is parameterized by its path length s. The parentheses $< \ldots >_s$ indicate an

average around the ring and $\eta(s)$ is the periodic dispersion. On the design orbit of a separated function ring, which HERA-e is to a good approximation, $G(s)\cdot K(s) = 0$ around the ring and since $\eta(s)\cdot G(s) \ll 1$ one has $J_x \approx 1$, $J_s \approx 2$.

Shifting the RF frequency from f_c to $f_c + \Delta f$ changes the momentum of the closed orbit particles in a first order approximation by $\delta = \frac{\Delta p}{p_0} = \frac{\Delta f}{f_c}/(\frac{1}{\gamma^2} - \alpha_p) \approx \frac{1}{\alpha_p}\frac{\Delta f}{f_c}$, with the momentum compaction factor $\alpha_p \gg \frac{1}{\gamma^2}$. The closed orbit is therefore shifted by $\eta\delta$ and therefore has curvature in quadrupoles. The momentum shift also changes the curvature in dipoles, the focusing strength, and the dispersion somewhat:

$$G_\delta \approx G(1-\delta) + K\eta\delta \ , \quad K_\delta \approx K(1-\delta) \ , \quad \eta_\delta \approx \eta + \delta\partial_\delta\eta \ . \tag{7}$$

For a separated function ring these changes lead to

$$\mathcal{D}_\delta = \mathcal{D} - \frac{1}{\alpha_p}\frac{< 2\eta^2K^2 + (\partial_\delta\eta - \eta)G^3 >_s}{< G^2 >_s}\frac{\Delta f}{f_c} \ . \tag{8}$$

Since the $G^3 \ll \eta K^2$ in strong focusing rings like HERA, the damping partition numbers become zero as follows:

$$J_s = 0 \quad \text{for} \quad \Delta f = f_c\alpha_p\frac{< G^2 >_s}{< \eta^2K^2 >_s} \ , \tag{9}$$

$$J_x = 0 \quad \text{for} \quad \Delta f = -\frac{1}{2}\Delta f_s \ . \tag{10}$$

At these frequency shifts the emittances diverge and the lifetime becomes zero. Increasing the RF frequency from f_0 to f_+ and decreasing it to f_- where the lifetime is reduced from several hours to some minutes can therefore be used to determine the central frequency by

$$f_c = \frac{1}{3}(2f_- + f_+) \ . \tag{11}$$

In first order approximation the width of the damping window is $\frac{3}{2}f_c\alpha_p\frac{<G^2>_s}{<\eta^2K^2>_s}$ and is independent of Energy. Simulations with MAD yielded the following separations of damping poles: in the current 60° optics 2170Hz and for the new 72° optics 2290Hz.

When shifting the RF frequency, the beam can be lost due other reasons than reaching the damping poles. For example the closed orbit, which follows the dispersion function, could come close to an aperture limitation. The lifetime was recorded as a function of frequency shifts for four different settings of HERA-e, and the two extreme frequencies were taken as f_+ and f_-. These four settings were the following: the current luminosity optics with 60° phase advance per FODO cell at 27.5GeV (obtained Jan. 9, 1999), the current injection optics at 12GeV (Mar. 13, 1999), the new 72° injection optics at 12GeV and at 27.5GeV (Dec. 19, 1998), and the new 72° luminosity optics at 27.5GeV (Dec. 20, 1998). The by γ^2 increased emittance at 27.5GeV causes the drop in lifetime to be less abrupt than at 12GeV, and it therefore is best to measure at low energy. However, even at low energy the lifetime is measured to be zero before the RF frequency is exactly at the damping pole. The frequency error relative to the distance from the damping pole can roughly be estimated as follows: After recent repairs at electron dipole

magnets in January 1999, the horizontal dynamic aperture should be around 13σ at 27.5GeV. The lifetime is measured to be zero when the dynamic aperture is about 5σ of the beam emittance. Therefore, the lifetime at 12GeV is measured to be zero when $1/1 - \mathcal{D} = (13/5)^2 \cdot (27.5/12)^2$ and therefore when $\mathcal{D}$ is about 1/30 smaller than 1. This corresponds to a relative distance of 3% from the damping pole. This estimate also shows why the drop of lifetime with frequency is much more sudden at 12GeV than at 27.5GeV, as can be observed in figure 19. A similar estimate can be obtained for the longitudinal damping pole at 12GeV. Here the relative energy spread at injection is $\sigma_\delta = 4 \cdot 10^-4$ and the relative bucket height at $94MV$ cavity voltage per turn is $\Delta E/E_0 \approx 4$. This leads to $2/2 + \mathcal{D} = (10^4/5)^2$ and the lifetime is measured to be zero at a RF frequency shift which is approximately $3 \cdot 10^{-5}\%$ too small.

Figure 19 shows all data points taken. The extremest frequencies are $f_+ = f_0 + 1830\text{Hz}$ and $f_- = f_0 - 670\text{Hz}$ leading to a central frequency f_c which is 163Hz above the current operation frequency f_0.

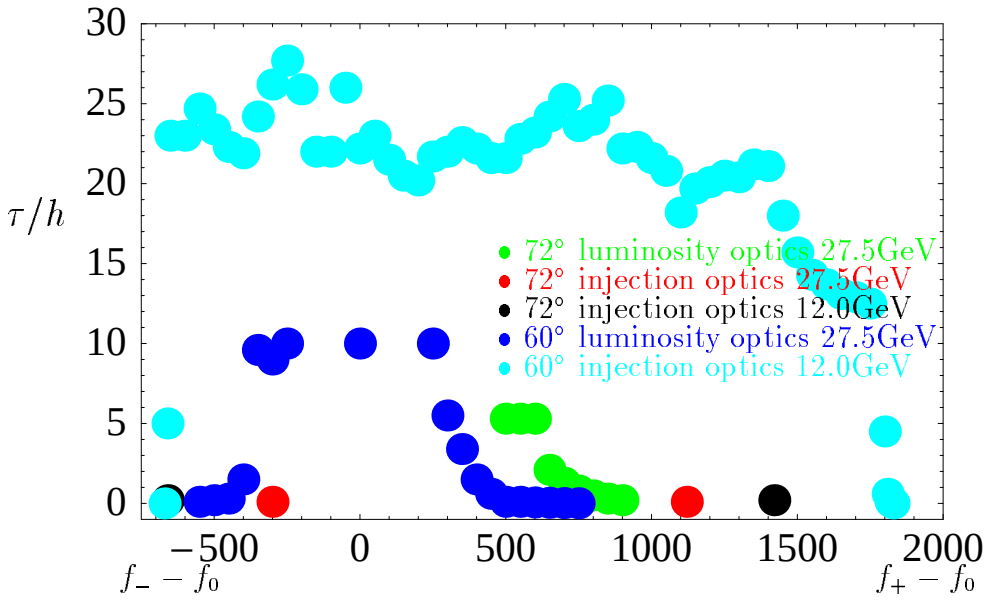

Figure 19: Lifetime as a function of RF frequency shift Δf relative to the current operation frequency f_0 for four different machine settings. The extreme frequency shifts occurred at 12GeV in the 60° optics. The data are consistent with a central frequency which is 163Hz above the current operation frequency.

6.2 Measurement of the Center Frequency in the HERA Electron Ring

Date: 1998, Dec. 16, 7am–11am, Logbook XXXIV, page 150–153

The foreseen luminosity increase in the luminosity upgrade project of HERA is partially based on optimizations of the lattice and transverse beam optics of both the electron and the proton machine, as described in the HERA upgrade study. Another part of the enhancement factor however is due to a change in the frequency of the electron storage ring which leads to a redistribution of the damping partition numbers which will lead to a smaller horizontal emittance of the electron beam.

Supposed the center frequency of the machine is known it can be shifted by a dedicated amount to achieve the foreseen effect. The center frequency is established if the corresponding closed orbit is running through the center of all magnetic elements, namely the quadrupole and sextupole magnets. In this context mainly the sextupole magnets are of interest.

6.2.1 Procedure of the Measurement

For the measurement a stored electron beam at injection energy was used. Tune controller and feed-back system were switched off, the tune indicator however was active as for the procedure the tune measurement was needed. The frequency of the 500 MHz rf-system was shifted slowly and the resulting change of the horizontal and vertical tune was measured.

The same measurement was repeated after changing the strength of all sextupole magnets in the ring by a small amount. The resulting tune values, plotted again as a function of the frequency change, will have a different ascent: The particles running off center through the sextupole magnets will be affected by the stronger or weaker focusing strength of the 'off-center sextupole lenses'. At the center frequency however the closed orbit is expected to pass without offset through the sextupoles and the different strengths of these magnets will have no effect on the tune. So the measured tune values will be the same even if the sextupole strengths had been changed.

6.2.2 Result

In the figure the tune in the horizontal plane is plotted as a function of the frequency shift. The horizontal plane thus shows the difference of the applied frequency at the moment of the measurement with respect of the starting frequency, that was used during the run year before. The three curves represent the measured tune values for the standard sextupole settings and for a machine of 10% increased or 10 % decreased sextupole fields respectively. The straight lines are a least-square-fit through the data.

The tune lines cross at a frequency of

$$f_{centre} = -138.9 \pm 20 Hz$$

which means that the true center frequency found by the measurement is about 139 Hz lower than the frequency used in the present machine at that time. The error is deduced from the calculation of the crossing points of two lines respectively.

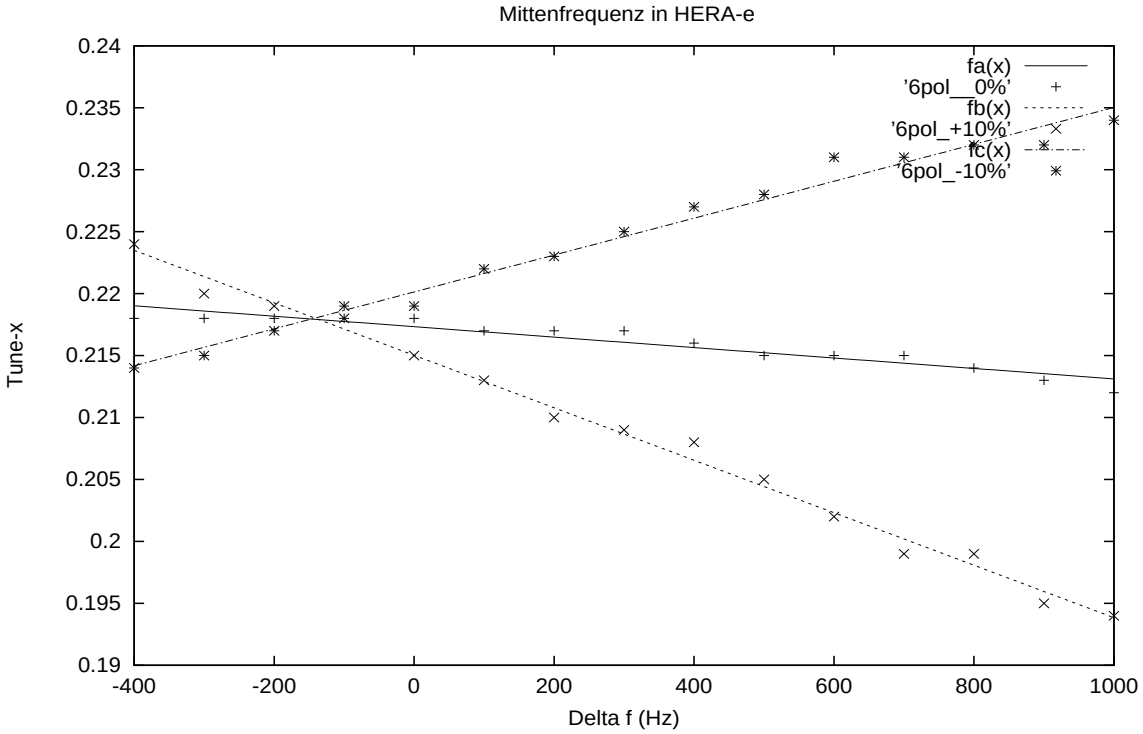

Figure 20: Measurement of the horizontal tune shift as a function of the changing RF-frequency. The crossing point of the fitted lines reflect the center frequency of the machine.

As the sextupole settings applied during the studies also affect the vertical tunes in the same way, the shift of the vertical tune was measured as well for completeness. Surprisingly enough the tune curves now are crossing at a slightly different '*center-frequency*'.

As shown in the next figure, the center frequency obtained from the vertical tune measurement is

$$f_{centre} = 102.8 \pm 49Hz$$

The frequency shift foreseen in the upgrade project of $\Delta f_{rf} = 350Hz$ is well within the stable range of the electron storage ring of HERA as can be seen in the above plotted figures. The difference in the measured center frequencies however is surprising. A possible explanation would be that the horizontal and vertical acting sextupole magnets are aligned in the ring with a substantial systematic offset in the horizontal plane with respect to each other.

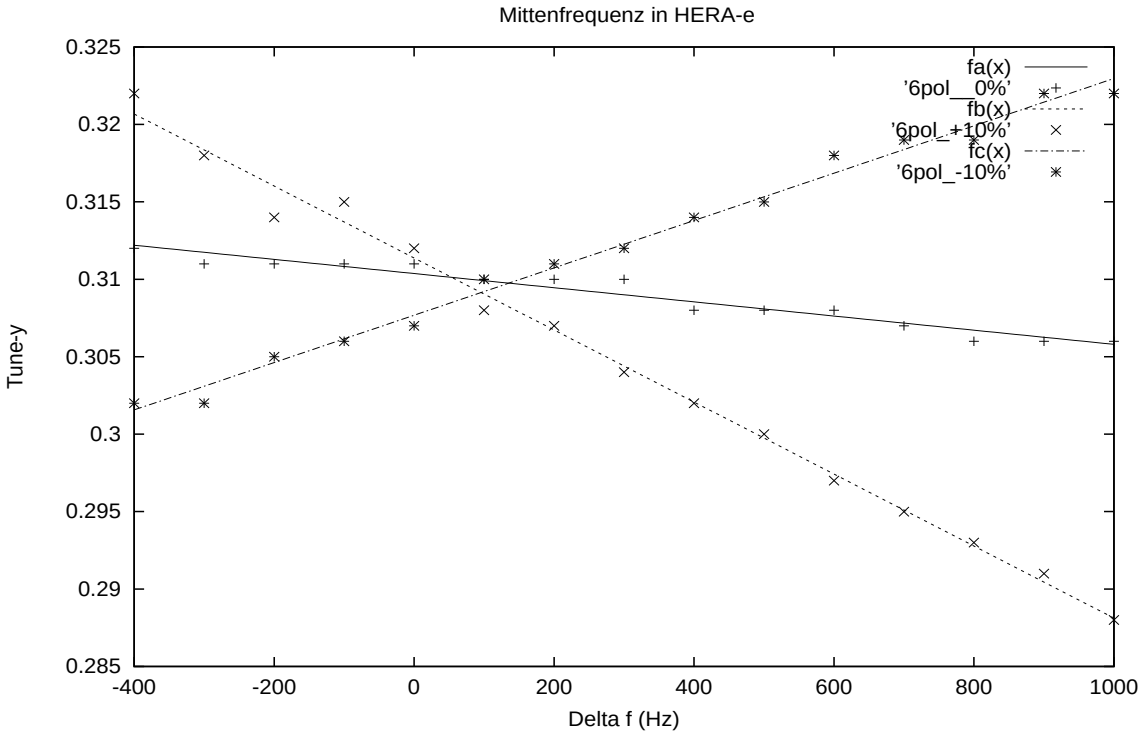

Figure 21: *Measurement of the vertical tune shift as a function of the changing RF-frequency.*

6.3 Measuring the Damping Partition of the HERA-e Beam

Date: 1998, Dec. 20, 11pm to Dec. 21, 7am Logbook XXXIV, page 203–212

Die Lage der Dämpfungspole des HERA Elektronenstrahls wurde bestimmt durch Messung der Abklingzeit kohärenter Schwingungen in der horizontalen Ebene bei verschiedenen HF Frequenzwerten. Die Extrapolation der Meßkurven $1/\tau$ versus $\Delta f/f$ nach $1/\tau = 0$ ergibt einen Frequenzkorrekturwert von etwa -620Hz gegenüber der jetzigen Arbeitsfrequenz. Daraus kann man schließen, daß der derzeitige Arbeitspunkt um mindestens 100Hz unter der Mittenfrequenz liegt.

6.3.1 Motivation

Verschiebt man die Frequenz des Beschleunigungssystems in einem (Kreis-) Beschleuniger, so zwingt man die Teilchen auf eine kürzere bzw. längere Bahn, die nicht mehr durch die Mitte der Quadrupolmagnete geht. Dies ist nur möglich, wenn sich gleichzeitig die Energie der Teilchen ändert. Die Dipolfeldkomponenten auf der verschobenen Bahn in den Quadrupolen schwächen oder verstärken die Stärke der Ablenkmagnete. Die Beziehung zwischen Energie- und Frequenzverschiebung ist $\Delta E/E = -(1/\alpha)\cdot\Delta f/f$. Hier ist α der momentum compaction factor $\alpha = \oint dsD/\rho$ (D: Dispersionsfunktion, ρ: Ablenkradius der Dipolmagnete).

Die Tatsache, daß die Gleichgewichtsbahn nicht mehr durch die Mitte der Quadrupole geht, hat für den Elektronenstrahl wichtige weitere Konsequenzen: Das Dämpfungsverhalten des Strahls wird nachhaltig beinflußt. Treten Dipol- und Quadrupolfelder an der gleichen Stelle auf, wie das bei einer verschobenen Gleichgewichtsbahn der Fall ist, so werden kohärente Schwingungen stärker bzw schwächer gedämpft und zwar so, daß die Summe der Dämpfungsraten aller drei Schwingungsebenen immer ein Konstante ist (Robinson Theorem). Die Dämpfungsverteilung auf die Schwingungsebenen wird durch die sogenannte 'damping partition number' $\mathcal{D}$ beschrieben, die im Falle einer 'separated function'-Maschine (Dipol- und Quadrupolmagnete aufeinanderfolgend) mit Energieverschiebung $\varepsilon = \Delta E/E$ durch folgenden Ausdruck gegeben ist:

$$\begin{aligned} \tau_i &= \tau_0/J_i \\ J_{hor} &= 1-\mathcal{D} \\ J_{vert} &= 1 \\ J_{long} &= 2+\mathcal{D} \end{aligned}$$

$$\mathcal{D} = \frac{\oint dsD/\rho^3 + 2\oint dsk^2D^2\varepsilon}{\oint ds/\rho^2}.$$

(τ_i: Dämpfungszeit auf der Mittenfrequenz für Modi i (hor,vert,long), k: Fokussierstärke der Quadrupolmagnete, i: hor., vert. oder long.). Der erste Term im Zähler der Dämpfungsverteilung ist klein gegen eins. Der zweite, energieabhängige Teil kann sehr leicht in die Grössenordnung von eins gelangen.

Die Dämpfung kann durch kombinierte Dipol- und Quadrupolfelder soweit verschoben werden, daß sich Dämpfung in Antidämpfung verkehrt. Der Frequenzverschiebung, bzw Energieverschiebung, bei der sich in einer Ebene die Dämpfungsrate null ergibt heißt Dämpfungspol. Es gibt einen longitudinalen Dämpfungspol und einen horizontalen Dämpfungspol (falls die Vertikaldispersion verschwindet).

Die Kenntnis der Lage der Dämpfungspole ist wichtig für das Verständnis der Strahlemittanzen und des Aperturbedarfs der Elektronenmaschine. Passen die Hochfrequenz und der Maschinenumfang nicht zusammen, so ergibt sich eine Verschiebung der Dämpfungsverteilung und damit eine Abweichung der horizontalen Emittanz vom Designwert. Bei HERA bewirkt bereits eine Bahnverlängerung von nur $2mm$ eine Emittanzvergrösserung um 20%. So kleine Bahnverlängerungen können mit Mitteln der Vermessung nicht mehr bestimmt werden. In der Nähe der Dämpfungspole (das heißt schon vor Erreichen des Pols) wird der Aperturbedarf der Maschine größer als die Akzeptanz und die Strahllebensdauer ist null. Deshalb kann die genaue Lage der Pole durch eine Lebensdauermessung nur schwierig bestimmt werden. (Siehe dazu auch den Abschnitt von G. Hoffstätter zu diesem Thema).

6.3.2 HERA Parameter

Die Messungen wurden bei einer Strahlenergie von 27.5GeV durchgeführt. Die benutzte Strahloptik war die Standard Optik mit einem Phasenvorschub von $60grd$ pro FODO-Zelle (HEINJ). Der Momentum Compaction Factor in dieser Optik beträgt $\alpha = 6.4 \cdot 10^{-4}$. Die Dipolmagnete in HERA haben eine Länge von $L = 9.185m$ und besitzen einen Ablenkradius von $\rho = 608m$. Die Dispersion in den Quadrupolen beträgt $D_{foc} = 0.8m$, $D_{defoc} = 0.3m$. Die Ablenkstärke der Bogenquadrupole beträgt $kl = 1m^{-2}$. Die HERA HF beträgt $\simeq 500MHz$. Die nominalen Dämpfungszeiten (d.h. bei null Energieverschiebung, bei der sogenannten Mittenfrequenz) betragen $\tau_{hor} = 14.3ms$ und $\tau_{long} = 6.45ms$ (1/e-Zeiten). Mit diesen Parametern werden die Dämpfungspole bei ca -900Hz und +1800Hz Frequenzabstand von der Mittenfrequenz erwartet.

6.3.3 Messungen

Es wurden insgesamt 3 Bunche mit einem Strom von ca 0.5mA gefüllt. Der Strahl wurde bis 27.5GeV beschleunigt.

Die Chromatizität betrug zu diesem Zeitpunkt etwa $\xi_{x,y} \simeq 1$. Zum Zeitpunkt der Messungen stand nur eine horizontale Anregungsmöglichkeit zur Verfügung. Der Strahl wurde mit dem Injektionskicker 4 gekickt und Schwingungen mit einer Anfangsamplitude von etwa 2.8mm (1.8mm) angeregt. Dies entspricht einer Spannung U am Pulser von 0.6kV (0.4kV). Die Schwingungen wurden mit einem transversalen Monitor beobachtet, der für das transversale Dämpfersystem benutzt wird. Die Schwingungen wurden mit einem Digitaloszilloskop aufgezeichnet. Als Maß für die Dämpfungszeit wurde die Halbwertszeit der Envelope bestimmt (unter Benutzung der Cursor Funktionen am Scope). Der Strahllagemonitor zeigte bei den relativ großen Schwingungsamplituden ein Einschwingungsverhalten mit einer Zeitkonstante von ca. $(1-2)ms$. Es wurde darauf geachtet, daß diese Einschwingvorgänge die Bestimmung der Abfallzeit nicht verfälschen (nur der zeitlich

Table 3: Meßdaten

Meßreihe 1, U=0.4kV			Meßreihe 2, U=0.6kV		
Δf	τ_{damp}	$1/\tau_{damp}$	Δf	τ_{damp}	$1/\tau_{damp}$
[Hz]	[ms]	[kHz]	[Hz]	[ms]	[kHz]
579	8.88	0.112613	1679	4.92	0.203252
679	9.16	0.10917	1579	6.44	0.155280
779	7.76	0.128866	1479	6.04	0.165563
879	8.56	0.116822	1379	7.00	0.142857
979	8.56	0.116822	1279	7.92	0.126263
1079	7.04	0.142045	1179	7.64	0.130890
1279	6.76	0.147929	1079	7.96	0.125628
1479	5.6	0.178571	979	8.68	0.115207
1679	5.12	0.195313	879	9.2	0.108696
1879	4.08	0.245098	779	9.56	0.104603
1909	3.56	0.280899	679	8.08	0.123762
			579	8.08	0.123762

nach dem Einschwingungsvorgang liegende Bereich der Schwingungen wurde verwendet). Es wurden zwei Meßreihen (U=0.6kV, U=0.4kV) durchgeführt, wobei die HF Frequenz jeweils im Bereich von $\Delta f_{hf}/f_{hf}$ = 579Hz....2000Hz variiert wurde. Der Wert von 579Hz entspricht dem jetzigen Arbeitspunkt. Die Meßwerte sind in Tabelle 3 aufgelistet.

Die Meßpunkte bei extrem großen Frequenzverschiebungen befinden sich bereits recht nahe am Dämpfungspol. Daher trat während der Meßzeit schon merklicher Strahlverlust auf, der aufgrund der Eigenschaft des Schwingungsmonitors die Meßwerte möglicherweise beinflußt.

6.3.4 Auswertung und Diskussion

Die Abbildung 22 zeigt die Zerfallsraten der horizontalen Schwingung als Funktion der Frequenzverschiebung. Die Werte sind korrigiert um einen Beitrag von Landaudämpfung.

Es wird erwartet, daß die Meßpunkte auf einer Geraden liegen, welche die Gerade $1/\tau_{damp} = 0$ am horizontalen Dämpfungspol schneidet.

Die horizontale Dämpungszeit bei 27.5GeV in HERA beträgt laut PETROS 9.9 ms (Halbwertszeit, on-energy). Das entspricht 472 Umläufen. Der Strahlungsdämpfungsmechanismus steht in Konkurenz mit anderen Zerfallsprozessen einer kohärenten Schwingung wie zum Beispiel Landaudämpfung oder Kohärenzzerfall durch Chromatizität. Die Landaudämpfungszeit (aufgrund der Nichtlinearität der Sextupole wird mit 2000-3000 Umlaufszeiten abgeschätzt [3]. Mit diesen Werten, die einer Dämpfungsrate von 0.025kHz entspricht, sollte die Landaudämpfung durch Sextupole das Ergebnis nicht nennenswert beeinflussen. Unter der Annahme, daß die Landaudämpfung sich der Strahlungsdämpfung multiplikativ überlagert wurden die gemessenen Dämpfungsraten um den Wert von 0.025kHz korrigiert.

[3]Formeln aus: F. Willeke, FNAL TM1309 5-1985, unter Verwendung der Werte $Q_x = Q_{x0} + A_x x^2 + A_y y^2$, $A_x = 11m^{-2}$; $A_y = 133m^{-2}$ (für nominale Sextupolfelder aus Brinkmann/Willeke DESY 86-079) $\sigma_x = 1.3mm$, $\sigma_y = 0.35mm$, $x_0 = 2.8mm$ @ $U_{kick} = 600V$

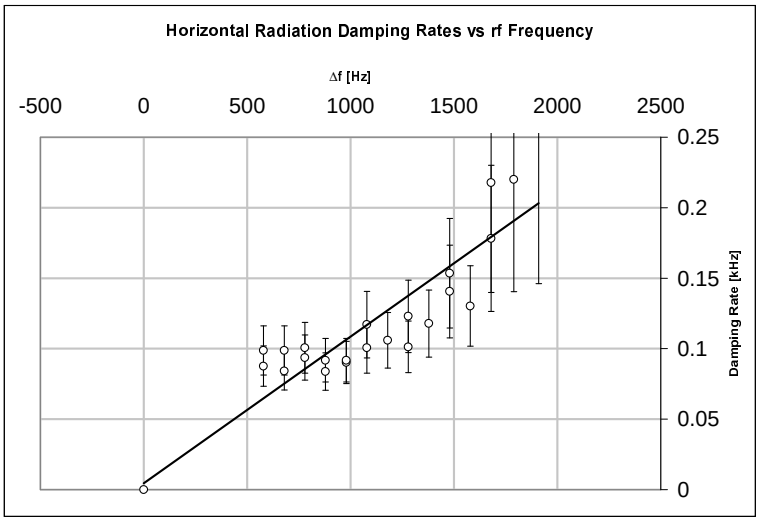

Figure 22: Radiation Damping Raten als Funktion der HF Frequenzverschiebung. Die Rate sind korrigiert um einen konstanten Beitrag von 0.025kHz, der von der Landaudämpfung abgeschätzt wurde. Der Meßfehler der Dämpfungszeit wurde mit 1ms abgeschätzt.

Die Tune-Verteilung aufgrund der Chromatizität beträgt 10^{-3}. Aufgrund der kurzen Synchrotronperiode von nur ca 20 Umläufen spielt der Kohärenzzerfall durch Chromatizität jedoch keine Rolle (die Betatronphasenbeziehungen zwischen den Teilchen sind jeweils nach einer Synchrotronperiode wieder restauriert).

Es ist unschwer zu erkennen, daß die Punkte in Abbildung 22 nicht auf einer Geraden liegen. Bei den größten und kleinsten Frequenzwerten weichen die Meßpunkte von der Geraden, die man durch die Meßpunkte in der Mitte legen kann ab. Für die Meßpunkte oberhalb 1800Hz bietet sich der Strahlverlust aufgrund der Nähe zum longitudinalen Pol als Erklärung an. Bei kurzen Abklingzeiten spielt möglicherweise auch die Zeitkonstante des Monitors eine Rolle. Für die Abweichung der Meßpunkte von einer Geraden bei kleinen Frequenzwerten bietet sich keine offensichtliche Erklärung an. Man muß also wohl die Meßfehler verantwortlich machen. Fittet man eine Gerade an alle Meßpunkte an, so schneidet diese Gerade die Frequenzachse bei $-50\text{Hz}\pm \simeq 150\text{Hz}$. Dies entspricht dem horizontalen Dämpfungspol. Der Abstand vom Pol zur Mittenfrequenz sollte 900Hz betragen. Damit erwartet man den Dämpfungspol bei (850 ± 150)Hz. Der Meßwert der Dämpfungszeit (korrigiert um die Landaudämpfungszeit, Wert auf der Ausgleichsgeraden bei 850 Hz) beträgt bei dieser Frequenz 15ms (1/e-Zeit). Dies entspricht sehr gut dem Erwartungswert von PETROS (14.3ms). Damit liefert die Messung zwar ein nicht sehr genaues aber immerhin im Rahmen der Fehler konsistentes Ergebnis. Die derzeitige Arbeitsfrequenz von HERA-e liegt bei einem Frequenzoffset von 579Hz und sollte nach dieser Messung ca $(270 \pm 150)Hz$ unter der Mittenfrequenz liegen.

6.3.5 Ausblick

Es sollte auch eine longitudinale Dämpfungsmessung durchgeführt werden. Dazu muß eine longitudinale Anregung geschaffen werden.

7 Coupling Measurements in HERA-e

Date: 1998, Dec. 15, 3pm–11pm Logbook XXXIV, page 145–148

In 1991 a tilt of the beam ellipse of about 8 degrees at 12 GeV was observed at the synchrotron light monitor. The tilt increased with energy.
In HERA-e there are no skew quadrupoles: the effect was (and it is) corrected by the "decoupling bump", which produces a vertical offset at a large number of sextupoles and thus a skew field. This cure suggests that the coupling source itself is distributed.
This year the question arose whether a new localized source of coupling existed. Indeed, by trying to minimize the vertical oscillations at injection, one could observe a blow up of the vertical oscillation amplitude approximatively at the IP North.
Some experiments were done to analyze this problem.

7.1 Observations

One of the observations was to measure the minimum tune separation when the beam ellipse tilt was minimized by the decoupling bump. The measured tune distance was not larger then 280 Hz (i.e. $Q_x - Q_z \simeq 0.006$).

A second set of measurements was to observe the change of the horizontal and vertical closed orbit occurring when a correction coil is turned on. These observations have been repeated by using one after the other three consecutive coils in the regular FODO cells. There was no effect of vertical coils on the horizontal orbit, whereas for a $\Delta x_{rms} \simeq 1.85$ mm, a $\Delta z_{rms} \simeq 0.15$ mm at most was observed (the "noise" of the orbit measurement is usually responsible for a Δz_{rms} of about 0.05 mm). An analysis of the collected data with the SVD method is planed.

The last set of observations was done during electron injection by looking at the first turn oscillations. Here the advantage is that the sextupoles may be turned off, thus eliminating a source of non-linearities.

A first turn trajectory was recorded and compared with those obtained when horizontal correction coils just behind the injection region were turned on. One could observe a blow up of the vertical oscillation amplitude as shown in figure 1. However, when the sextupoles are switched off, there is no clear correlation between horizontal and vertical motion as shown in figure 2.

The fields due to sextupoles are given by

$$B_x = sxz = sx_o z_o + sx_o z_\beta + sz_o x_\beta + sx_\beta z_\beta \tag{12}$$

$$B_z = \frac{1}{2}s(x^2 - z^2) = \frac{1}{2}s(x_o^2 - z_o^2 + 2x_o x_\beta - 2z_o z_\beta + x_\beta^2 - z_\beta^2) \tag{13}$$

Since the vertical closed orbit z_o is non-zero (and/or the sextupoles may be displaced vertically), an extra radial field is generated at the sextupoles when the horizontal betatron oscillation x_β change. A simulation shows that the observations are quantitatively in rough agreement with this simple explanation.

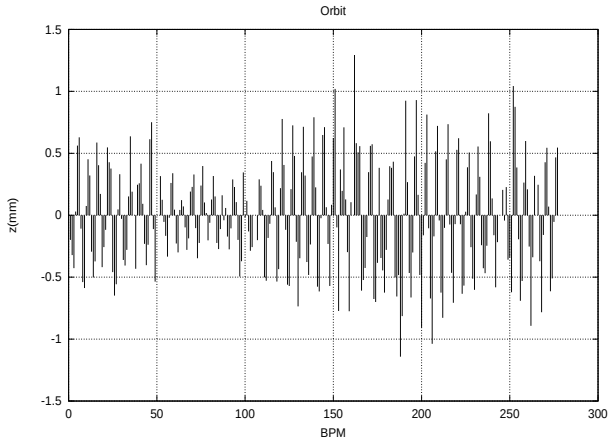

Figure 23: Vertical oscillation change by a 0.150 mrad horizontal kick; the 50th BPM is the first BPM after injection. Electrons move from left to right.

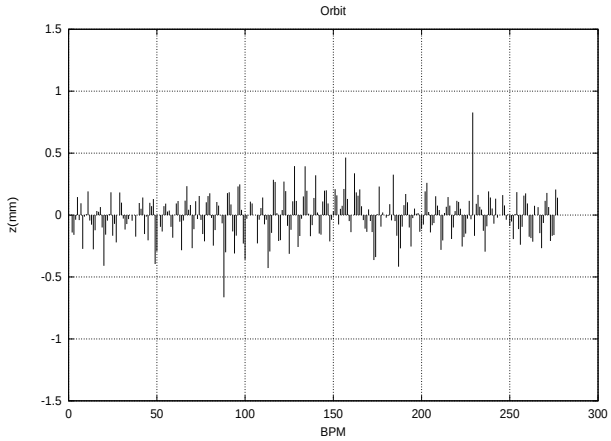

Figure 24: Vertical oscillation change by a 0.150 mrad horizontal kick with sextupoles off; the 50th BPM is first BPM after injection. Electrons move from left to right.

7.2 Summary

I would conclude that no evidence for a local source of coupling was found.

8 Testing the Beam Beam Tune Shift Limit for Protons at HERA

Date: 1998, Dec. 10, 7am to Dec. 11, 7am Logbook XXXIV, page 104–118
1998, Dec. 13, 11pm to Dec. 14, 7am Logbook XXXIV, page 132–136

In the framework of the HERA Luminosity Upgrade Project the beam sizes in the interaction regions will be reduced. This results in an increase of the beam beam tune shift. The effect of the increased tune shift on the proton beam has to be tested. With the present optics of the HERA interaction regions a higher tune shift for the protons can be reached by increasing the electron bunch population.
The electron filling scheme for this test and the measurement procedures will be presented. Due to several beam losses during the tests no results were obtained.

8.1 Introduction

The present optics of the HERA interaction regions leads to horizontal and vertical beam beam tune shifts for the protons of $\Delta\nu_{xp} = 0.0007$ and $\Delta\nu_{yp} = 0.0002$ per interaction point, respectively. In 1997 higher electron currents were reached and the tune shifts went up to $\Delta\nu_{xp} = 0.0011$ and $\Delta\nu_{yp} = 0.00028$. The HERA luminosity [5] upgrade will result in smaller spot sizes at the interaction points and therefore, when the design electron current of 56mA is achieved, in increased tune shifts of $\Delta\nu_{xp} = 0.0017$ and $\Delta\nu_{yp} = 0.0006$. The influence of such high tune shifts on the lifetime and the emittance of the proton beam has to be investigated.

8.2 Theory

The theory of the beam beam tune shift can be found in a paper by H. Mais and C. Mari [3]. For an electron proton collider the horizontal proton tune shift per interaction region is given by

$$\Delta\nu_{xp} = \frac{\beta_{xp} r_p N_e}{2\pi\gamma_p(\sigma_{xe} + \sigma_{ye})\sigma_{xe}}.$$

Here β_{xp} is the horizontal beta function of the protons in the interaction point, r_p is the classical proton radius, N_e is the number of electrons per bunch, γ_p is the relativistic γ factor of the protons, σ_{xe} and σ_{ye} are the horizontal and vertical spot sizes of the electrons in the interaction point, respectively. Table 4 shows the tune shifts for a standard electron fill of 30mA in 189 bunches with the current luminosity optics and for a 56mA fill after the luminosity upgrade.

For the test run it was foreseen to fill electron bunches with up to $5.3\ 10^{10}$ electrons per bunch, resulting in tune shifts of $\Delta\nu_{xp} = 0.0018$ and $\Delta\nu_{yp} = 0.00047$.

	HERA 1998	HERA 2000
β_{xp}	7 m	2.45 m
β_{yp}	0.5 m	0.18 m
r_p	1.5 10^{-18} m	1.5 10^{-18} m
N_e	2.1 10^{10}	3.9 10^{10}
γ_p	980.81 GeV	980.81 GeV
σ_{xe}	200 μm	118 μm
σ_{ye}	54 μm	32 μm
$\Delta\nu_{xp}$	0.0007	0.0017
$\Delta\nu_{yp}$	0.0002	0.0006

Table 4: Proton beam beam tune shifts: currently and after the lumi upgrade with design electron currents.

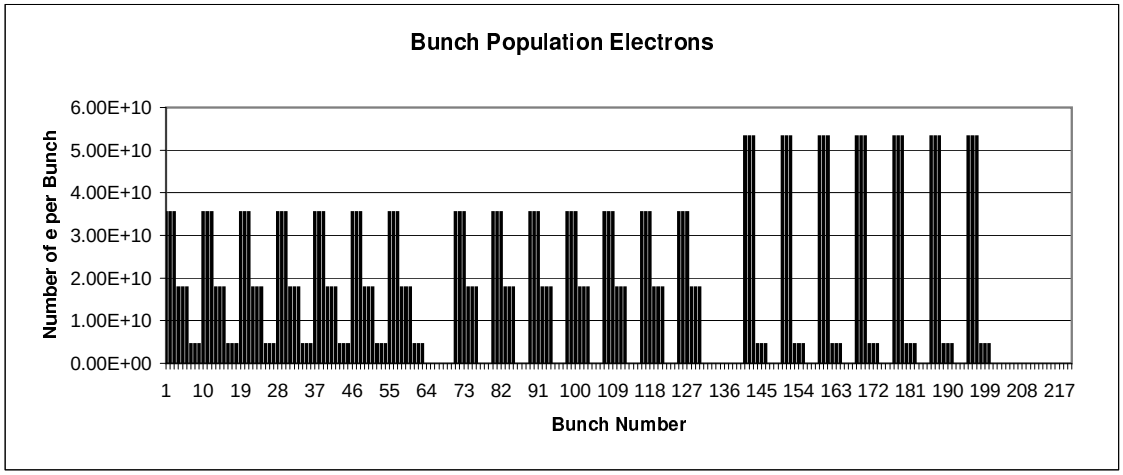

Figure 25: Electron Bunch Population

8.3 Filling Scheme

A standard luminosity fill with 5.3 10^{10} electrons per bunch, as foreseen for the test run, would lead to a total electron current of 75mA, which today is beyond the capability of the HERA electron ring. As at the time of the measurement due to technical limitations the total electron current was limited to 30mA, only a few bunches with bunch populations up to 5.3 10^{10} could be filled.

I order to avoid strong beam loading effects in the rf cavities, resulting in potential technical problems with the longitudinal electron feedback, the electron bunch charge in HERA has to be distributed more or less evenly around the ring. Therefore, besides the bunches with high bunch charge needed for the test run, some smaller bunches have to be filled in between, so that the total charge is well distributed around the ring.

Figure 25 shows the electron bunch population chosen for the test runs.

8.4 The Measurement

The beam beam tune shift measurements were scheduled for December 10 to 11, 1998 and had to be continued until December 14. The protocol can be found in the log book HERA ep XXXIV, pages 104 ff.

Due to several technical problems, which were not related to the measurements or the unusual electron bunch population, it was not possible to achieve colliding beams before December 14, 5.30 AM.

The procedure to prepare the measurements was much like for a normal luminosity run:

First some 80mA protons in 180 bunches were filled and accelerated to 920GeV. Afterwards the emittance of several selected proton bunches (see below) was measured with the wire scanner. For this purpose the wire scanner was switched to single bunch mode (SEM mode) and the bunches were selected using a console application found under
S:Projects/Vb/Wscanner/Btmwsc/Wscbtm.exe

In order to determine the lifetime of the selected bunches, the number of protons per bunch was measured using the oscilloscope 3 (HE11) in average mode (average 20). In addition the lifetime of one bunch (#142) was measured using the proton bunch mountain range display of Mr. Kriens and Mr. Hurdelbrink.

Then, as the electrons were filled in the usual steps, the electron bunch population was adjusted according to the following scheme:

Step	Anzahl	Bunches	Current/3Bu. μA	Electr./Bunch	Current/Step mA
1	7	21	800	$3.55\ 10^{10}$	5.6
2	7	21	800	$3.55\ 10^{10}$	5.6
3	7	21	1200	$5.32\ 10^{10}$	8.4
4	7	21	400	$1.77\ 10^{10}$	2.8
5	7	21	400	$1.77\ 10^{10}$	2.8
6	7	21	100	$0.44\ 10^{10}$	0.7
7	7	21	100	$0.44\ 10^{10}$	0.7
8	0	0	0	0	0
9	0	0	0	0	0
Sum		147			26.6

Table 5: Filling Scheme for the Electrons.

The electron tune controller was set on bunch #159, a high current electron bunch colliding with a proton bunch which was not used for the measurements. After the electrons were accelerated to 27.5GeV, luminosity was established and optimized using the usual procedures. During this run HERA-B was asked not to use the target wires, the beam position at Hermes was not optimized, and ZEUS and H1 were asked to switch on the luminosity monitors, but to leave off all sensitive detector components, because the frequent use of the wire scanner produced spikes in the background rates.

Figure 26 shows the electron and proton bunch population used during the one successful luminosity run.

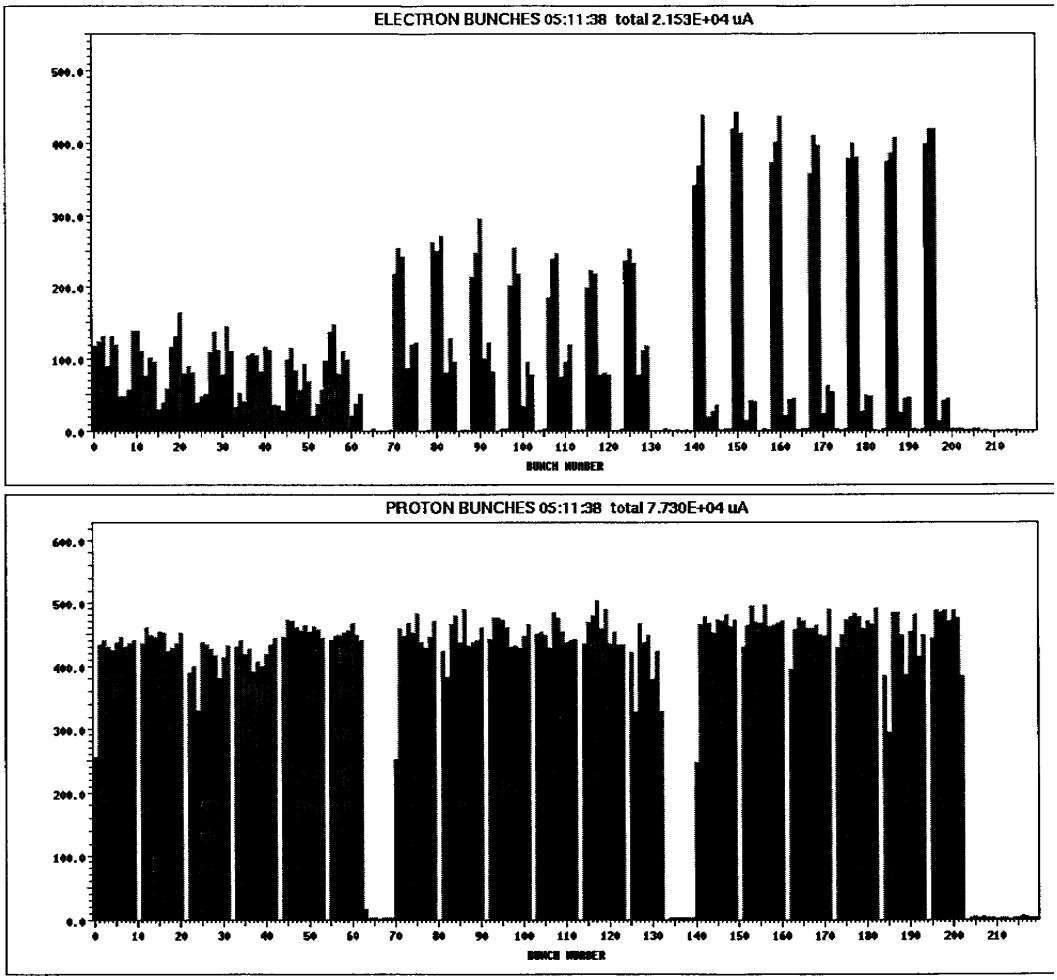

Figure 26: Electron and Proton Bunch Population

p-Tuneshift for selected Bunches:

Bunch	Prot./Bunch	E-Step	Electr./Bunch	p-Tuneshift (x)	p-Tuneshift (y)
126	5.171E+10	2	3.55E+10	0.00119	0.00032
127	5.171E+10	2	3.55E+10	0.00119	0.00032
129	5.171E+10	5	1.77E+10	0.00060	0.00016
130	5.171E+10	5	1.77E+10	0.00060	0.00016
132	5.171E+10	8	0.00E+00	0.00000	0.00000
133	5.171E+10	8	0.00E+00	0.00000	0.00000
142	5.171E+10	3	5.32E+10	0.00179	0.00048
143	5.171E+10	3	5.32E+10	0.00179	0.00048
145	5.171E+10	6	4.44E+09	0.00015	0.00004
146	5.171E+10	6	4.44E+09	0.00015	0.00004

Table 6: Tune Shifts for selected Proton Bunches

For the measurements a number of proton bunches were selected, colliding with electron bunches of different charge, resulting in different tune shifts. Table 6 shows the bunch numbers and the expected tune shifts.

During the luminosity run the following parameters were continually measured:

- Specific Luminosity
- Proton lifetime
- Lifetime of selected proton bunches
- Emittance of selected proton bunches

Unfortunately the measurement ended after just 30 minutes due to a technical problem which caused a beam loss. The data do not allow to calculate any lifetimes and there were no indications for different behavior of proton bunches colliding with strong or weak electron bunches.

After the end of the measurements a leak in the waveguide system of the 1GHz transmitter for the longitudinal electron feedback system was detected. Figure 27 shows the damaged waveguide. Due to the very non-symmetric electron bunch distribution the longitudinal feedback system was operated at a higher power level than usual. As the cavities of the feedback system are operated in an unmatched mode, reflections into the waveguide are possible and might have caused the damage. Now a light detector has been installed in the waveguide and connected to the interlock system, so that the transmitter will be switched of in case of arcs in this waveguide section.

8.5 Summary

The tests have proven that it is possible to fill and accelerate a very non-symmetric electron bunch distribution. Due to other technical problems the actual time for measurements under luminosity conditions was too short to draw any quantitative conclusions about the effect of an increased beam beam tune shift on the protons. It can only be said that on the time scale of 30 minutes no effects became visible.

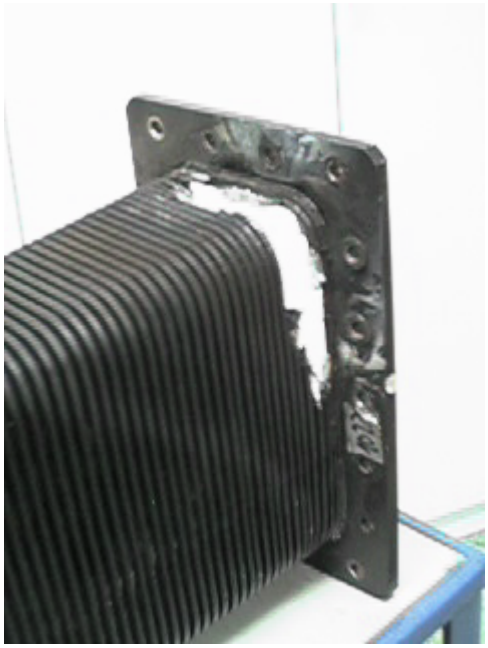

Figure 27: Damaged Waveguide of the 1GHz Feedback System

A. Budsko, O.R. Jones, M. Wendt

9 "Head-Tail" Phase Shift Measurements at Hera-p with Chirp Excitation

Date: 1998, Dec. 12, 7am to Dec. 13, 11pm Logbook XXXIV, page 129–132

A new method for a quasi non-destructive measurement of the chromaticity in HERA-p was tested. It is based on the detection of the phase difference of two longitudinal positions within a single bunch, after swept frequency (chirp).

9.1 Introduction

At present the *chromaticity* in HERA-p is measured by sweeping the rf frequency and measuring the resulting changes in the betatron tunes. Although this procedure was improved recently to allow a reliable result to be obtained within a few seconds, is does not allow the chromaticity to be measured during the energy ramp. Here we describe a method that allows the chromaticity to be calculated after several hundred turns from the turn-by-turn position data of a single bunch after transverse excitation. This so-called *head-tail* chromaticity measurement [6] relies on the fact that for non-zero chromaticity a dephasing/rephasing occurs between the head and tail of a bunch, with a frequency equal to the synchrotron frequency. By measuring the turn-by-turn position data at two longitudinal positions in a bunch it is possible to extract the relative dephasing of the head and the tail, and so to determine the chromaticity.

Previous experiments at the CERN SPS accelerator and HERA-p (Summer 1998 machine shifts [7]) have used single kick excitation to produce the transverse beam oscillation necessary for the measurement. In HERA-p, however, the only kicker capable of providing sufficiently large oscillation amplitudes from a single kick is the injection kicker. It limits the measurement on the horizontal plane and tends to produce a beam break-up, and can even lead to a beam loss, when fired during the ramp. In order to measure the chromaticity in both the transverse planes and during the enegry ramp, a different excitation method was required. In this case this was achieved by adding a *swept frequency (chirp)* component, centred on the nominal betatron tune, to the excitation signal used for tune measurements.

9.2 The Head-Tail Principle

Assuming longitudinal stability, a single particle will rotate in longitudinal phase-space at a frequency equal to the synchrotron frequency. During this longitudinal motion the particle also undergoes transverse motion, which can be described by the change in the betatron phase, $\Theta(t)$, along the synchrotron orbit. If the whole bunch is kicked transversely, then the resulting transverse oscillations for a given longitudinal position within the bunch can be shown [6] to be given by

$$y(n) = A\cos\left[2\pi n Q_0 + \omega_\xi\,\hat{\tau}\,(\cos(2\pi n Q_s) - 1)\right] \tag{14}$$

where n is the number of turns since the kick, Q_0 is the betatron tune, Q_s is the synchrotron tune, $\hat{\tau}$ is the longitudinal position with respect to the centre of the bunch, and ω_ξ is the chromatic frequency and is given by

$$\omega_\xi = Q' \omega_0 \frac{1}{\eta} \tag{15}$$

Here Q' is the chromaticity, ω_0 is the revolution frequency and $\eta = 1/\gamma^2 - 1/\gamma_{tr}^2$. If we now consider the evolution of two longitudinal positions within a single bunch separated in time by $\Delta\tau$, then from (14) it follows that the phase difference in the transverse oscillation of these two positions is given by

$$\Delta\Psi(n) = -\omega_\xi \, \Delta\tau \, (\cos(2\pi n Q_s) - 1) \tag{16}$$

This phase difference is a maximum when $nQ_s = 1/2$, i.e. after half a synchrotron period, giving

$$\Delta\Psi_{\max} = -2\,\omega_\xi \, \Delta\tau \tag{17}$$

The chromaticity can therefore be written as

$$\begin{aligned} Q' &= \frac{-\eta \, \Delta\Psi(n)}{\omega_0 \, \Delta\tau \, (\cos(2\pi n Q_s) - 1)} \\ &\text{or} \\ Q' &= \frac{\eta \, \Delta\Psi_{\max}}{2\,\omega_0 \, \Delta\tau} \end{aligned} \tag{18}$$

9.3 Experimental Procedure

9.3.1 Hardware Setup

Figure 28 shows the hardware setup placed in HERA Halle West. The transverse displacement signal of the proton beam was detected with the two horizontal 40 cm long stripline electrodes of the WR10m beam position pickup ($\beta \approx 33$ m). Their signals were adjusted in time with a variable delay-line and combined in a broadband Δ/Σ-hybrid. Additional fixed and variable attenuators were used to minimize the common mode signal due to the static beam displacement, i.e. the transverse beam orbit. Both output signals of the hybrid, Δ (displacement) and Σ (intensity), were acquired with a *Tektronix* 784C digital oscilloscope (1 GHz analogue bandwidth, 4 GS/s sampling rate). The Σ signal was used in the off-line post-processing of the signals to reduce the effect of jitter in the trigger signals. The necessity of this second signal channel limited the sampling rate to 2 GS/s. The oscilloscope was set to "fast-frame" mode, which allowed the capture of the signals for up to 372 consequtive turns [4]. Each "frame" covered 25 ns, with 50 sample points spaced by 500 ps, giving the displacement vs. time of a single bunch.

The chirp excitation was started manually by pressing a button on the *Chirp Unit*. This opened a 100 ms gate which passes bunch synchronous turn-by-turn triggers for the oscilloscope. This signal was provided by the *HERA Intergrated Timing* (HIT) system. The chirp duration and its lower and upper frequencies were programmed by varying R-C combinations. The output signal was added to the

[4] or the 2nd, 4th or 8th multiple

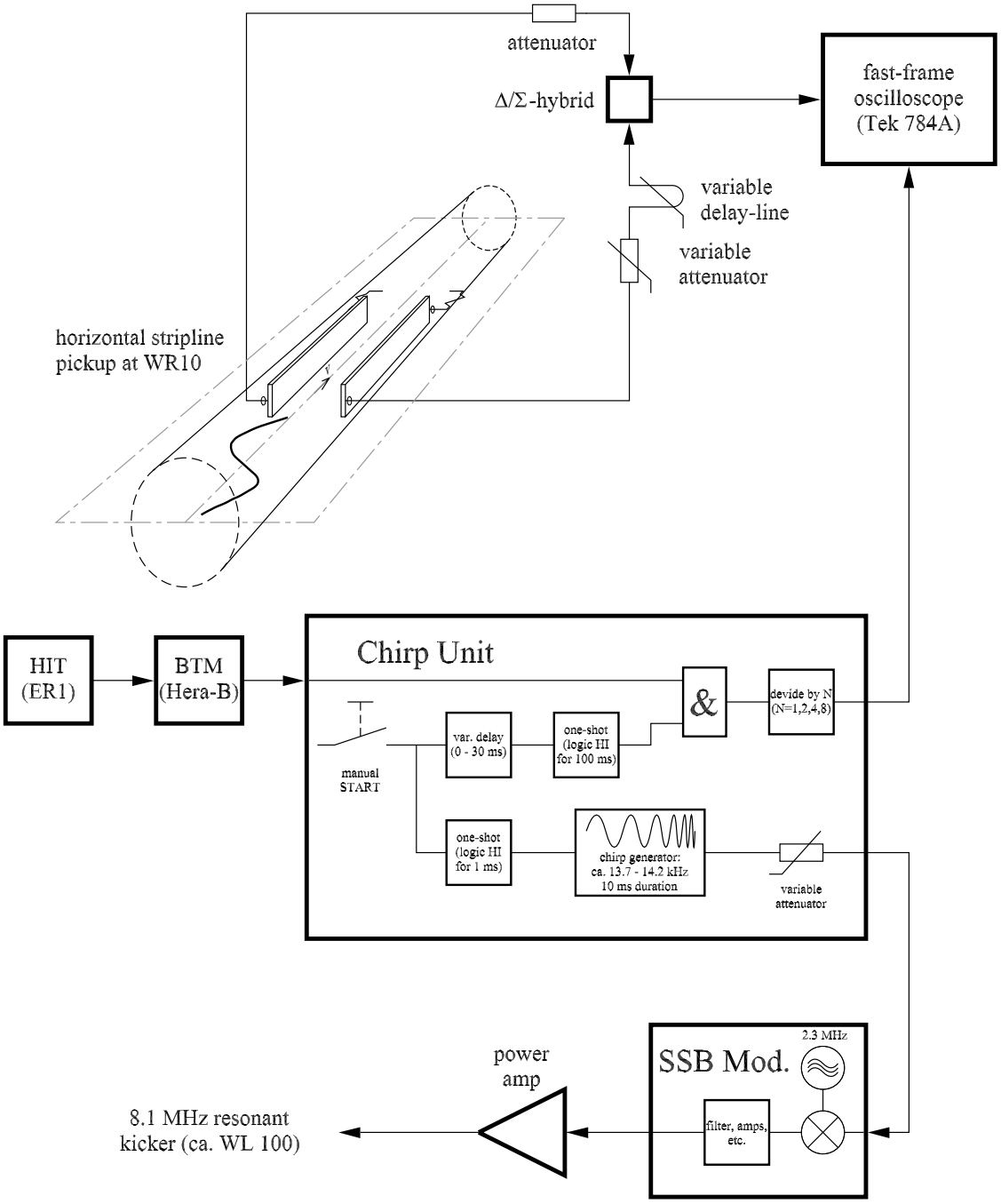

Figure 28: Hardware setup for the chromaticity measurements with chirp excitation.

SSB modulator of the resonant excitation kicker of the betatron tune measurement system.

The oscilloscope was PC-controlled via GPIB. A HP-VEE program dumped the data of all 372 frames automatically into an Excel spreadsheet and stored it with a time-stamp. The PC was also used for a brief off-line analysis of the data.

9.3.2 Shift Operations

The experiments were carried out during 5 shifts on the weekend 12/13 December, 1998. (logbook XXXIV, pp. 129-132)

The first early shift was used to set up the hardware and increased the excitation signal path to the resonant kicker by 30 dB. By adjusting the frequency range of the chirp generator to 13.7...14.2 kHz a strong reaction of the beam (total loss) was obtained.

During the late shift we the parameters of the chirp generator were fine-tuned. For this set-up period HERA-p was operatedn 40 GeV with 10 proton bunches at 40 GeV injection energy. The best values for the chirp turned out to be:

duration: 10 ms $\equiv$ 500 turns

frequency range: 13.5...14.5 kHz $\equiv$ 0.285...0.31

Throughout the night shift chromaticity measurements were carried out at 40 GeV injection energy under the following conditions:

- 10 bunches (4...5 mA beam current total)
- a set of 3 chirp measurements per sextupole (chromaticity) setting
- 7 chromaticity settings in the range -10...+10 units

Every set of measurements was made with fresh (new injected) beam. For comparision each sextupole setting was measured before and after the 3 chirp measurement using the "classic" method available in the control room. No beam breakup or losses were observed, but a reduced lifetime was noticed during chirp excitation (τ-plot: see logbook).

In the following shifts the beam was ramped in energy. Again 10 bunches were used, with measurements being taken before the start of each ramp file (at 70, 150 and 300 GeV), as well as during the ramp. A chirp measurement above 300 GeV proved to be difficult to achieved, due to the weak excitation level at this energy, and the tendency of the beam to break up for negative chromaticities. In case of a "break-up" we observed an increase of the bunch length (*times* 2) of the BPM signal on our oscilloscope.

At the end of our studies we tried to measure the synchrotron tune Q_s at different energies (40, 70, 150 and 300 GeV). As this procedure was not prepared, it did not prove successful and hence we have relied on theoretical values for all the resulting analysis.

9.4 Data Analysis

Since the sampling clock of the digital oscilloscope used in these experiments could not be synchronised to the turn-by-turn bunch trigger, it was necessary to sample both, the Σ and Δ signals from the hybrid coupler. The Σ signal was then used to

re-align each frame and hence correct for this jitter. This frame-by-frame correction factor was be applied to the Δ signal before starting the analysis. The head and tail analysis times were chosen so as to be symmetrical about the bunch centre. The transverse positions at these times in the bunch were then estimated by linear interpolation of the two nearest sampling points. Having obtained a set of head and tail data, phase demodulation using Hilbert transformation was carried out to obtain the turn-by-turn head and tail phase relative to a reference frequency. This reference frequency was chosen to be the average betatron frequency calculated from the Fourier power spectrum of both the head and tail data. The choice of reference frequency is however not critical, since we are ultimately only interested in the phase difference between the head and tail. The chromaticity could then be calculated by applying Equation (18) directly to the phase difference between the head and tail.

9.5 Results

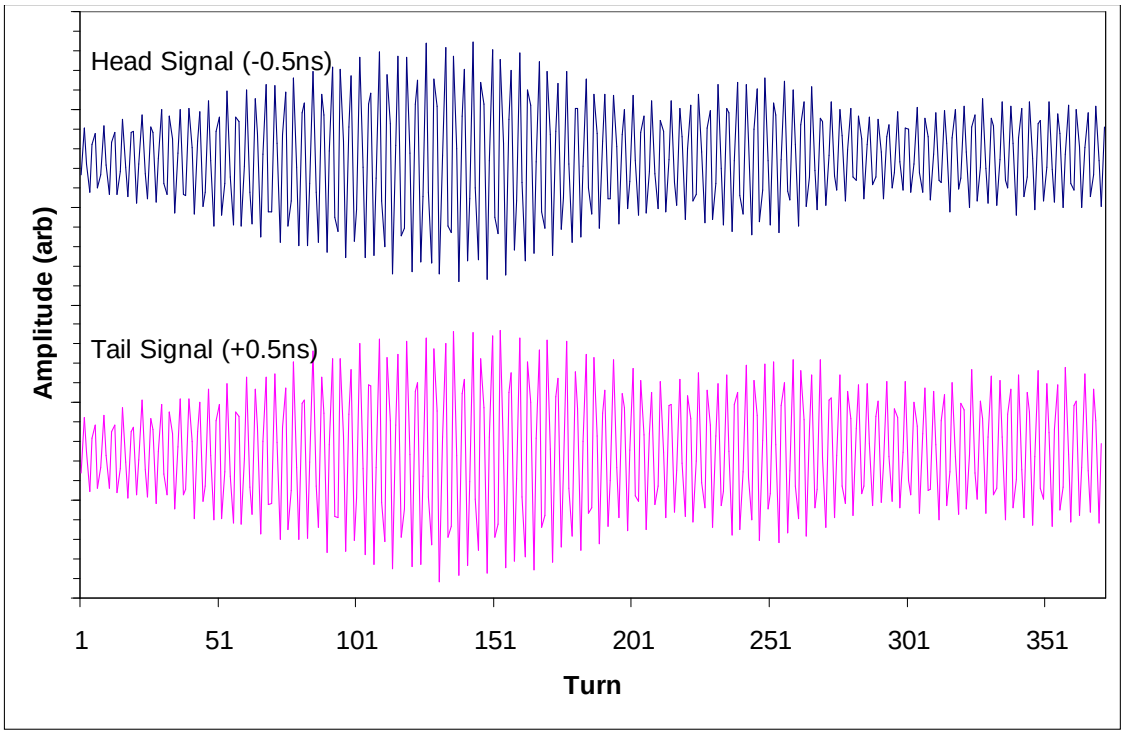

Figure 29: Transverse signals from the head and tail of a bunch after chirp excitation (70 GeV, horizontal chromaticity = +4).

Figure 29 shows the typical response of the head and tail of a bunch to chirp excitation. This is characterised by a growing oscillation amplitude followed by an amplitude "beating" for which the depth of the trough is a function of the width of the betatron tune peak and the rate at which the chirp is swept across the betatron resonance. The head and tail timing is relative to the centre of the bunch.

The dependence of the phase deviation on the longitudinal position of the head or tail is shown clearly in Figure 30. Here the swept "chirp" frequency crosses the betatron frequency at around turn 50, from which time the head and tail phases diverge from each other. What is also visible is that the response of the bunch to

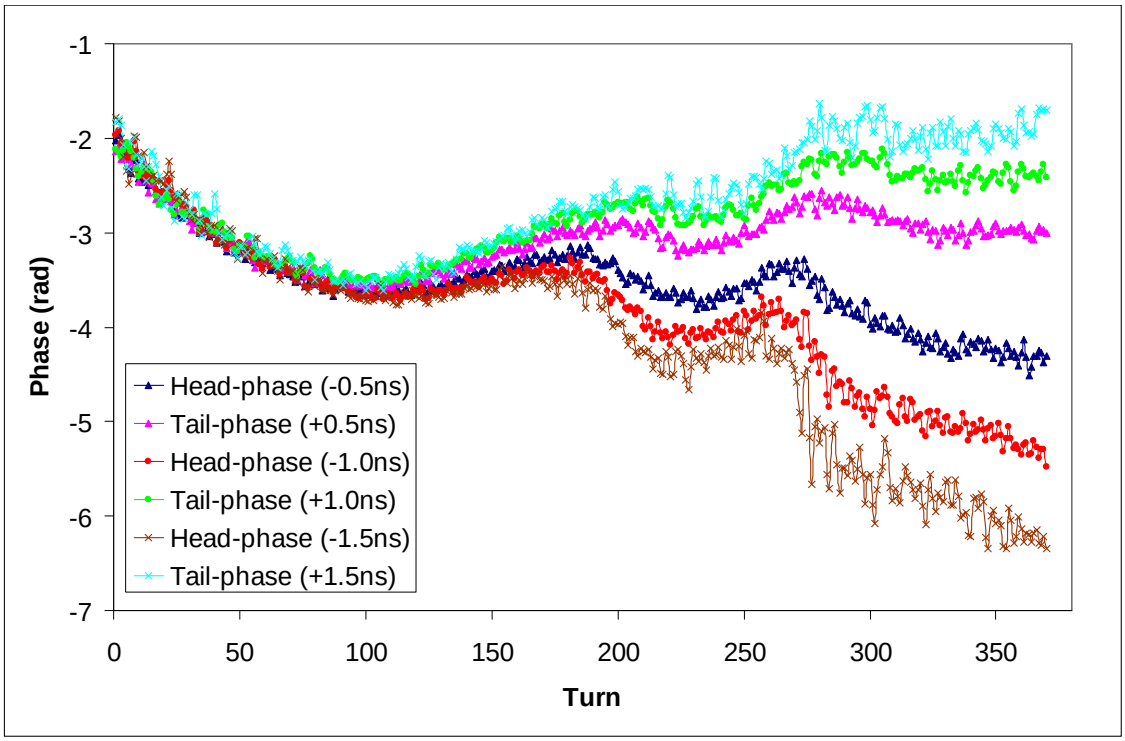

Figure 30: Phase evolution of several longitudinal positions within the same bunch relative to the centre of the bunch (70 GeV, horizontal chromaticity = +4).

the chirp itself produces a perturbation in the phase evolution. This proved to be a problem for certain chromaticities, where the troughs seen in Figure 29 went down to virtually zero, leading to large phase pertubations.

Figure 31 is the result of applying Equation (18) to the phase differences of the head and tail phases shown in Figure 30. By ignoring the perturbations caused by the chirp, the resulting chromaticity is seen lie between +3 and +5 units, which compares quite well with the +3 units measured by the BKR.

Figure 32 shows the result of two measurements performed at 300 GeV for positive and negative chromaticity. Again we see that the calculated chromaticities agree very well with the values measured in the BKR.

9.6 Conclusions

The results presented demonstrate the possibility of mesuring chromaticity using chirp excitation in less than 1000 turns, at energies up to 300 GeV. The main advantage of this technique over the current chromaticity measurement in HERA-p is that it can be performed during the energy ramp. Since only 15 % of the total available kick strength was used in obtaining these results, measurements at higher energies could be made possible simply by increasing the strength of the chirp signal. A beam break-up tendency during chirp excitation was observed at higher energies (¿ 300 GeV), but only for negative chromaticity.

Errors in the measured chromaticity were mainly due to the fact that the chirp was not synchronized to the data acquisition. This meant that the turn at which the chirp crossed the betatron frequency had to be estimated by eye from the phase evolution plots, which could lead to errors of up to ±2 units in the calculation of

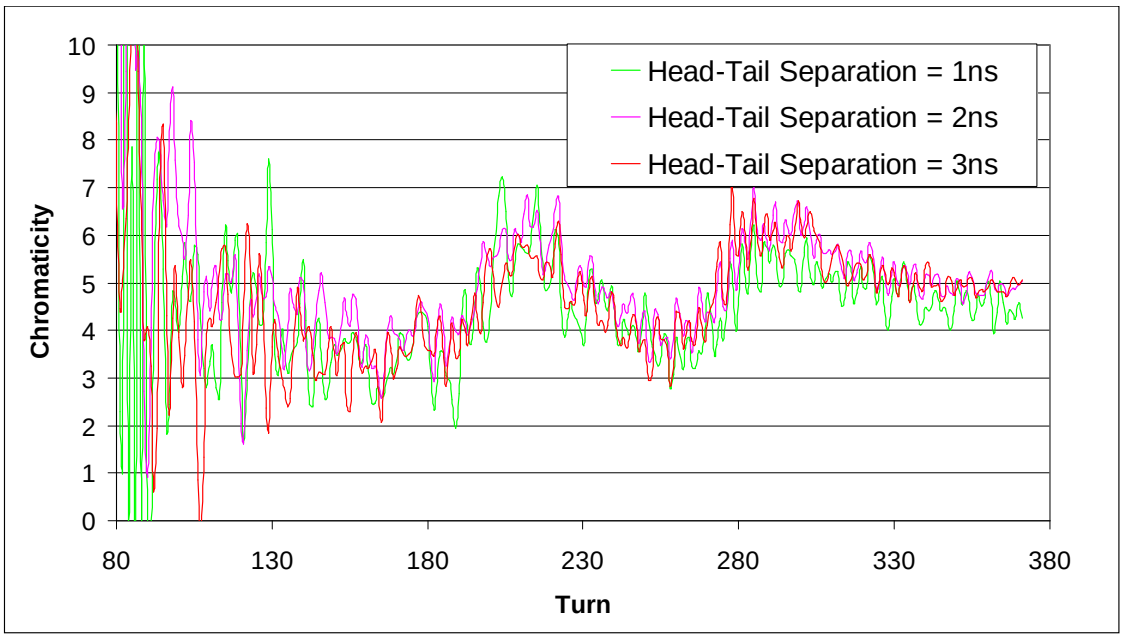

Figure 31: Turn-by-turn chromaticity for three different head-tail separations (70 GeV, horizontal chromaticity = +4).

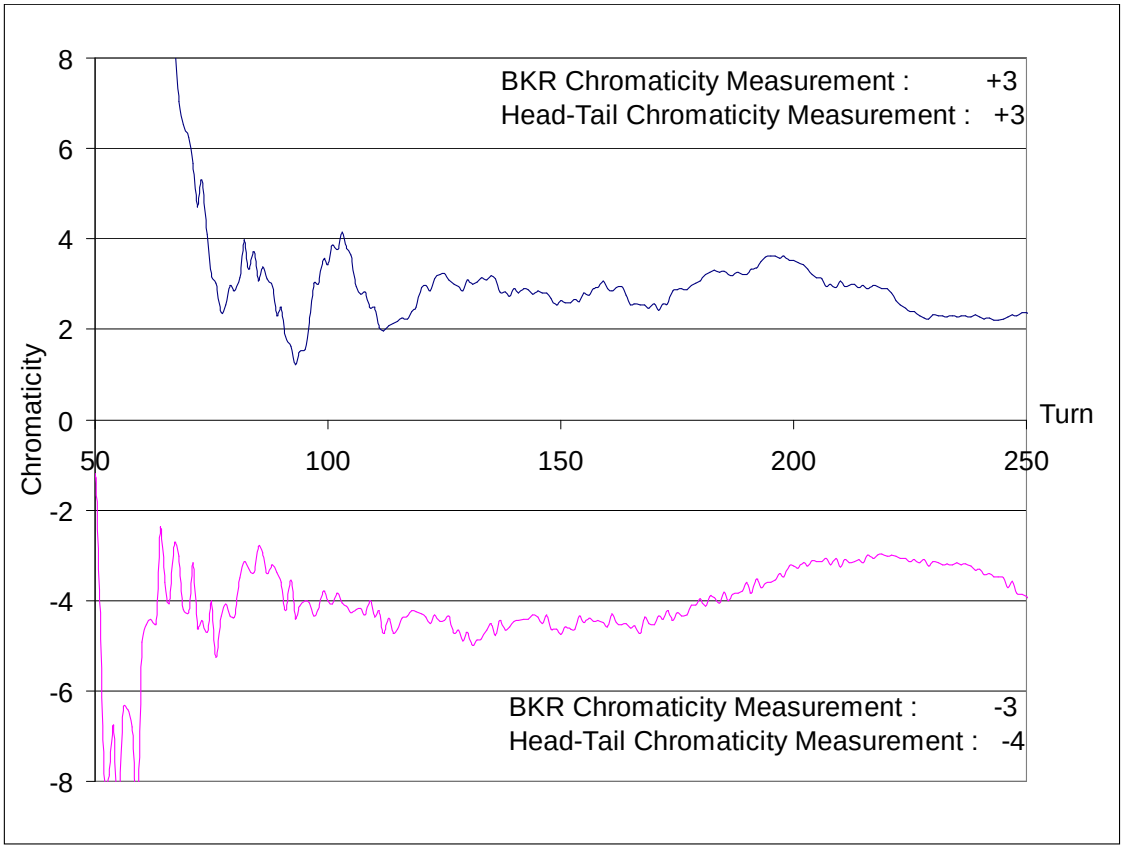

Figure 32: Turn-by-turn chromaticity for positive and negative chromaticity at 300 GeV.

chromaticity. Synchronising the chirp to the acquisition would allow the resonant tune to be calculated from the measured betatron tune and a knowledge of the chirp parameters.

10 Status and First Results of HERA-B Machine Studies

Date:	1998, July 13,	Logbook XXX,	page 248
	1998, Dec. 8, 7am–12am	Logbook XXXIV,	page 92
	1998, Dec. 9, 11pm to Dec. 10, 2am	Logbook XXXIV,	page 101–103
	1998, Dec. 14, 7am–7pm	Logbook XXXIV,	page 137–139

During machine studies in summer 1998 and in December 1998, investigations towards removing the coasting beam in HERA-p as well as some attempts to shape the transverse particle distribution have been carried out. This report summarizes the present status of these studies.

10.1 Coasting Beam

Since summer 1998, the HERA experiments suffer from a significant coasting beam contribution in HERA-p. Therefore the idea of removing this coasting beam by resonant dipole kicks within the dump kicker gap was brought up. The basic idea is to excite the coasting beam at its betatron frequency in order to finally remove it from the accelerator. This was tested during the machine studies in summer 1998 as well as in December 1998.

Regardless of the mechanism kicking particles out of the bucket, any unbunched proton will continuously lose energy due to synchrotron radiation, leading to a coasting beam contribution with negative momentum deviation. Therefore the coasting beam is expected to drift in the forward direction with respect to the bunched beam. Using the momentum compaction factor $\alpha_p = 1.3 \cdot 10^{-3}$ and the bucket height of $|\Delta p/p| = 2 \cdot 10^{-4}$ as the minimum momentum deviation of a coasting beam particle, the time to drift around the entire machine circumference relative to the bunched beam is about 80 sec. Obviously, this time decreases with increasing momentum deviation $\Delta p/p$. This means that a particle which is kicked out of the least bucket just in front of the dump kicker gap (bucket number 205) needs up to 80 sec to drift around the machine into the dump kicker gap where it can finally be removed by the kicker. During this drift process, the unbunched particles will continue to interact with the wire target, leading to further loss of energy and potential particle loss before reaching the dump kicker gap.

For technical reasons, the kicker frequency has to be modulated at $10.4\,\mathrm{MHz} = \frac{1}{96}\,\mathrm{nsec}^{-1} = N_b \cdot f_{\mathrm{rev}}$. Here $N_b = 220$ is the number of buckets and $f_{\mathrm{rev}} = 47.3\,\mathrm{kHz}$ is the revolution frequency.

As already mentioned above, an unbunched particle needs at most 80 sec to drift around the entire machine circumference. Therefore the time to drift over one kicker half period is just $80\,\mathrm{sec}/(2 \cdot 220) = 0.18\,\mathrm{sec}$, which corresponds to $0.18\,\mathrm{sec} \cdot 47300\,\mathrm{Hz} = 8600$ turns. Thus the drift of the coasting beam particles with respect to the bunched beam leads to an inversion of the kick direction after at most every 8600 turns, i. e. after receiving 8600 kicks leading to resonant excitation, the particles will be damped again by the following 8600 kicks if they are not lost at some

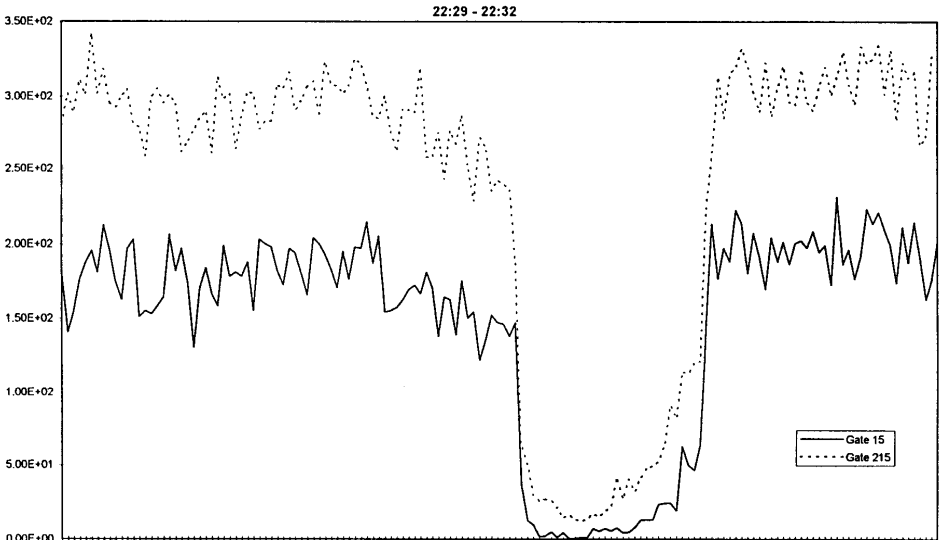

Figure 33: Measured HERA-B interaction rate versus time, ahead of (dashed) and behind (solid line) filled bunches with the target wire moving out and back in.

aperture limitation.
To study the feasibility of removing the coasting beam, 10 bunches with a total current of 3 mA were filled at positions 1 to 10 and ramped up to 820 GeV. The interaction rate with the HERA-B wire target was measured at the empty buckets 215 and 15, i. e. directly in front of and behind the filled buckets in order to determine the drift direction of the particles. Since the protons continue to interact with the wire target during their drift around the machine circumference, some fraction of particles gets lost at the target. Therefore an asymmetry in the drift direction leads to an asymmetry in the interaction rate ahead of and behind the bunches.
As figure 33 shows, the interaction rate with the target wire is significantly higher ahead of the bunches than behind, thus clearly indicating the "forward" drift direction. This drift direction corresponds to a negative energy deviation $\Delta p/p < 0$ of the coasting beam. As a next step, the horizontal feedback kicker was switched on. This led to an increased interaction rate at the excited (empty) bunch positions (fig. 34). This can be explained by a significant amount of coasting beam at a betatron amplitude not sufficient to reach the target wire, thus indicating an additional effect creating coasting beam.
Since the coasting beam could hardly be removed at 820 GeV, a second attempt was made at 40 GeV in order to check the principal feasibility of this scheme. This lower beam energy leads to a stronger effect of the feedback kicker, thus reducing the required number of kicks until the particle is finally lost. Unfortunately, due to extremely low target efficiency at that energy it was impossible to measure any coasting beam contribution, thus preventing this proof of principle.

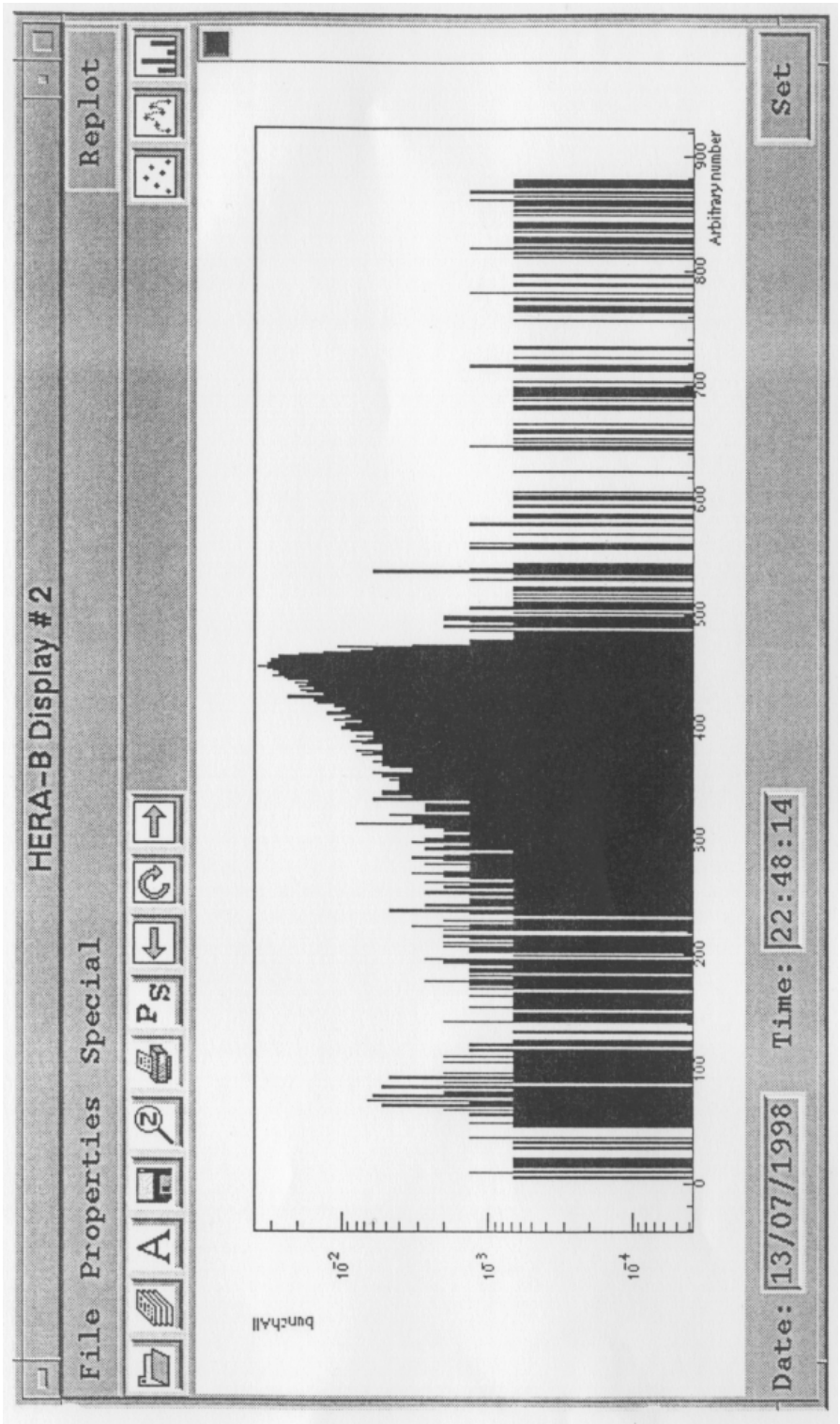

Figure 34: Measured HERA-B interaction rate with the kicker switched on. Each bucket is represented by four bins. Bunch 1 corresponds to bins 61 to 64, while the excited empty buckets 100 to 102 correspond to buckets 461 to 472.

10.2 Tail Shaping Using Dipole Kicks

10.2.1 Motivation

In a very simplified model, the motion of a particle in an accelerator with sextupoles is similar to a nonlinear oscillator, described by the differential equation

$$\ddot{x}(t) + \omega^2 x(t) - \epsilon x^2(t) = 0, \tag{19}$$

with initial conditions $x(0) = A$, $\dot{x}(0) = 0$. Obviously this simple model neglects the dependence of the potential on the longitudinal position in the accelerator, but nevertheless it illustrates the basic idea.
Solving this differential equation with the ansatz

$$x(t) = x_0(t) + \epsilon x_1(t) + \epsilon^2 x_2(t) + \ldots, \tag{20}$$

$$\omega^2 = \omega_0^2 + \epsilon\omega_1^2 + \epsilon^2\omega_2^2 + \ldots, \tag{21}$$

we get in second order perturbation theory

$$\begin{aligned} x(t) &= \frac{A^2\epsilon^2}{2\omega^2} - \frac{A^3\epsilon^2}{3\omega^4} \\ &\quad + \left(A - \frac{A^2\epsilon}{3\omega^2} + \frac{29A^3\epsilon^2}{144\omega^4}\right)\cos(\omega t) \\ &\quad + \left(\frac{A^3\epsilon^2}{9\omega^4} - \frac{A^2\epsilon}{6\omega^2}\right)\cos(2\omega t) \\ &\quad + \frac{A^3\epsilon^2}{48\omega^4}\cos(3\omega t), \end{aligned} \tag{22}$$

$$\omega^2 = \omega_0^2 + \frac{5A^2\epsilon^2}{6\omega_0^2}. \tag{23}$$

As equation (22) shows, such a nonlinear oscillator exhibits a spectrum of equally distributed frequencies $\omega_n = n \cdot \omega$, which become more and more dominant with increasing amplitude A.
Exciting the beam at a higher harmonic of the tune is therefore expected to result in a resonant behaviour of the protons, leading to an increased interaction rate at the HERA-B target wire.

10.2.2 Experimental Results

During the December 14th machine studies this was experimentally tested. A waveform generator was connected to the horizontal feedback kicker in the West area of the HERA proton ring. If we neglect any resonant behaviour of the beam, the maximum kick of about 32 nrad provided by the maximum integral magnetic kicker field of $1 \cdot 10^{-4}$ Tm at a location with $\beta_x = 240$ m results in a maximum orbit distortion of 1.3 μm at the HERA interaction points ($\beta_x = 7$ m). Since this orbit distortion is negligible compared to the 1σ beam size of 200 μm, this excitation should not result in any significant luminosity degradation.
After filling 26 mA in 60 bunches and ramping to 920 GeV, the inner target wire of the HERA-B experiment was moved towards the beam until an interaction rate of about 10 MHz was reached. At this position the target wire was fixed, and the

excitation at the third harmonic of the horizontal betatron frequency was switched on, the maximum integral kicker field being $0.4 \cdot 10^{-4}$ Tm. After tuning the excitation frequency in steps of 1 Hz, a significant increase of the interaction rate was achieved, as can be seen in the steep rise and fall off in the upper graph of fig. 35. Though this result seems to be promising, the effect on the beam core has to be checked with the wire scanner during future studies.

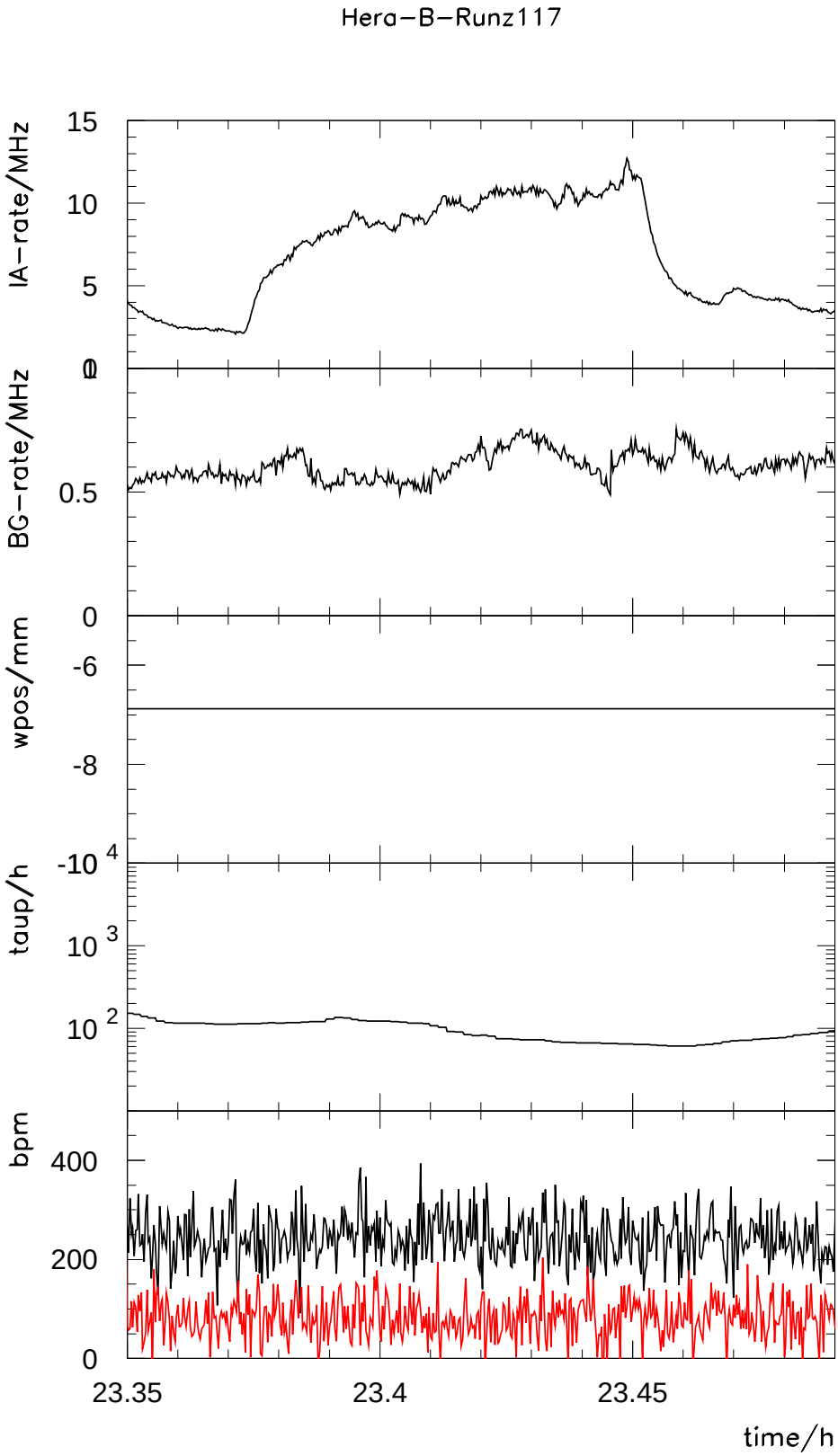

Figure 35: HERA-B interaction rate (IA-rate), background (BG-rate), target wire position (wpos), proton lifetime (taup) and beam position (bpm) after switching on the feedback kicker and some kicker frequency tuning (see text).

C. Kleffner, T. Limberg, F. Solodovnik, K. Wittenburg

11 Commissioning of a New PR–WeG Optics with a Split–Plane Quadrupole Magnet and a new Orbit Correction Program

Date: 1998, Dec. 11, 11pm to Dec. 12, 7am Logbook XXXIV, page 121–122

The injected proton beam in HERA must be horizontally focused at the injection point. The closer the last focusing element in the transport line can be moved towards the injection point, the smaller will the maximum β-function be at the end of the transport line "PR-Weg" and the bigger the acceptance. Fig. 1 is a sketch showing how an available split plane magnet quadrupole (named QMSQ) moved close towards the injection septum can be used to increase the acceptance in the injection region.

A resulting change in the geometry of the injection path stems from the fact that the beam in a split plane quadrupole magnet always experiences a net deflection. The quad has a k-value of 0.041 corresponding to a gradient of 5.5 T/m at 40 GeV beam energy. The aperture of the quad is a round beam pipe with an inner diameter of 54 mm. The beam travels 31.5 mm away from the magnetic center (if centered in the aperture) and is deflected 1.3 mrad by an integrated field of 0.17 Tm. This deflection has to be compensated by raising the strength of the near by septum magnet.

Acceptance Increase in the"PR-We"(Principle)

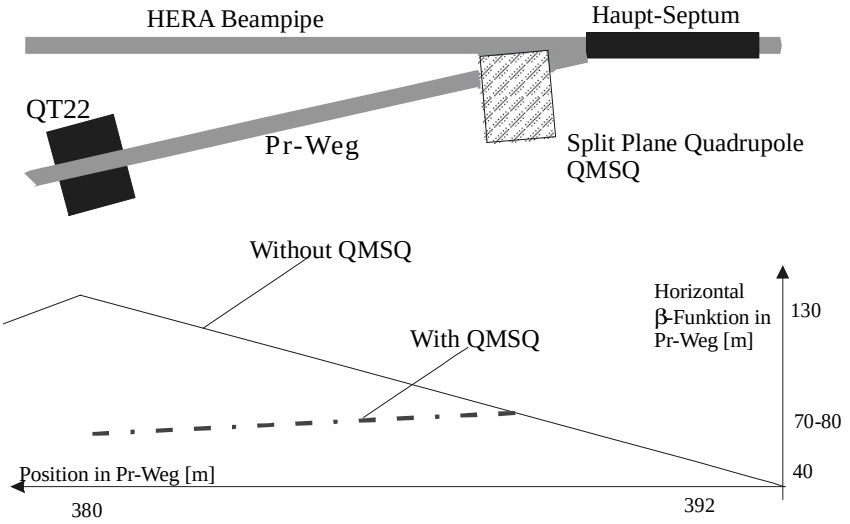

The Commissioning:

Within one shift the new optics using the QMSQ was dialed in and more than 95% transmission was achieved, although the "Haupt-Septum" could not be raised to the required strength due to technical problems. This is done now and transmission through the PR-Weg has been mostly undistinguishable from 100%.
Another 'fall out' from the injection optics change was a necessary change in the injection orbit correction standard procedure: two correctors and a septum magnet were originally used for correction in the horizontal plane. In the new PR-Weg optics the phase advance of one of the correctors to the septum becomes basically zero whilst the other moves closer to the favorable 90 degree value. Consequently, one of the correctors was removed from the correction algorithm.
Another goal of the shifts could not be achieved: Incoming quadrupole oscillations should be detected by a new wall current detector and subsequently minimized by adjusting the QMSQ and an optically orthogonal quadrupole. However, no clear signals of quadrupole oscillations could be seen due to high backgrounds although the QMSQ was varied over a wide range to a quarter of its original strength.

A new program was being tested to measure and correct the orbit in the PR-Weg. Fig. 2 shows a display of the program. On top two rows of buttons represent the screen monitors and the correction coils (horizontal plane in this case, selected in the leftmost box on top) which can be activated for orbit measurement and correction. Here three correctors are activated (shown green on display, dark gray on this plot) to apply a closed bump. The traces in the field below represent two horizontal orbit measurements. The dots are the positions of the centers of the beam images on the screens, the numbers on top and bottom the longitudinal position along the beam line in meters. Zero displacement is in the middle, the height of the window represents a maximum orbit displacement of +/- 10 mm. In the 3-bump region, the first orbit taken shows a peak deviation of -5mm, the dotted line is the suggested bump to correct for that. The bump has to be on top of the orbit to cancel the orbit offset! The other measurement shows the orbit after dialing the bump in; fairly good correction is achieved.
The pictures underneath the orbit window show at selected screens the beam profile and the center and a FWHM line from a gaussian fit as found by the code as well as reference values for these quantities. At the time being however, saturation effects of the optical system introduces large errors in the beam size measurements.

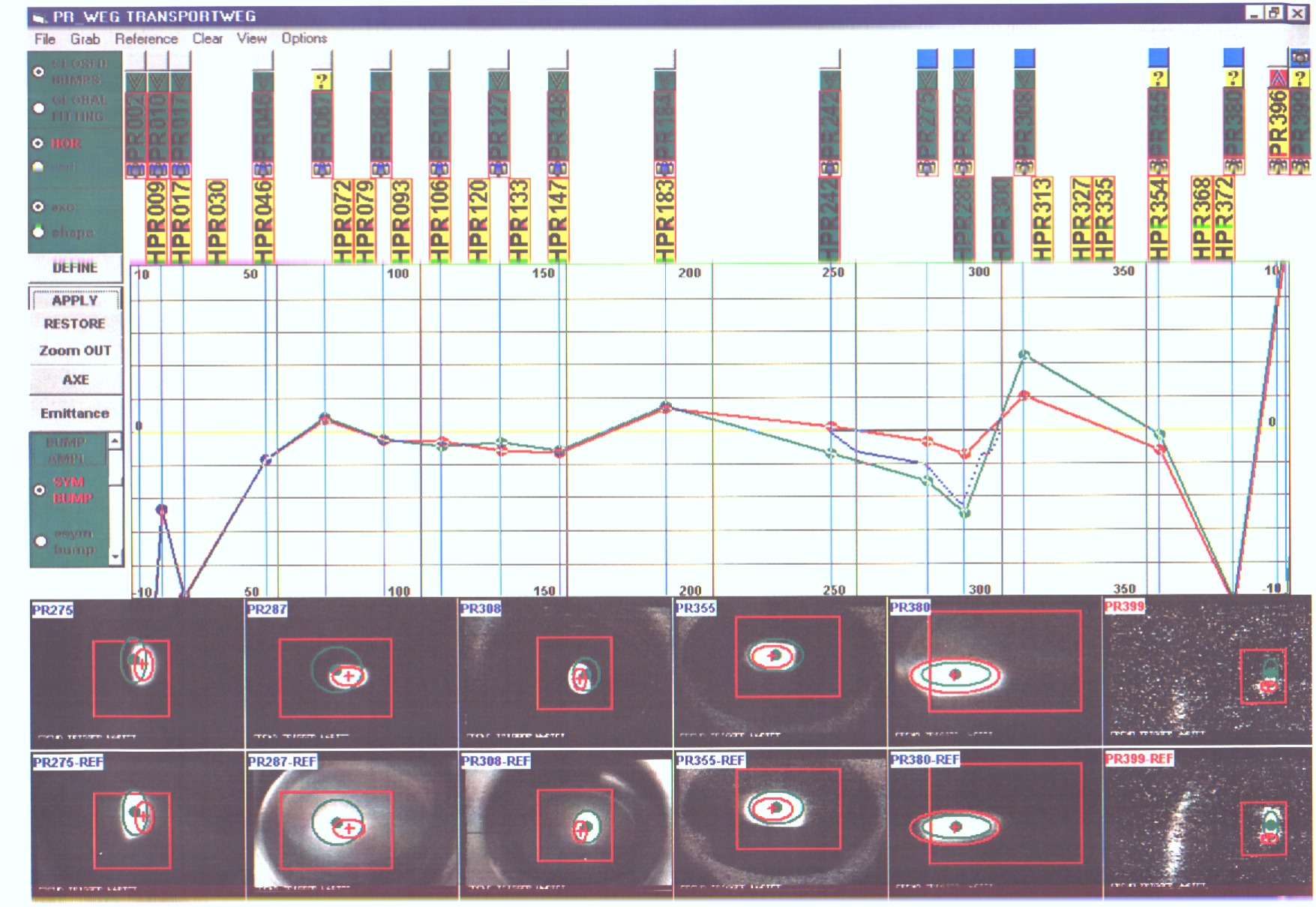
PR_WEG TRANSPORTWEG
File Grab Reference Clear View Options
CLOSED BUMPS
GLOBAL FITTING
HOR
VERT
exc
shape
DEFINE
APPLY
RESTORE
Zoom OUT
AXE
Emittance
BUMP AMPL
SYM BUMP
asym bump
HPR009 HPR017 HPR030 HPR046 HPR072 HPR079 HPR093 HPR106 HPR120 HPR133 HPR147 HPR183 HPR242 HPR313 HPR327 HPR335 HPR354 HPR368 HPR372
PR275
PR287
PR308
PR355
PR380
PR399
PR275-REF
PR287-REF
PR308-REF
PR355-REF
PR380-REF
PR399-REF

Acknowledgment: We emphatically thank F. Brinker, S. Choroba, M. Dohlus, U. Hurdelbrink, A. Joestingmeier, W. Kriens, M. Lomperski, and P. Wesolowski for there help, flexibility, and enthusiasm during the presented machine studies.

References

[1] Y. Alexahin, G. H. Hoffstaetter, and F. Willeke, Electron Dynamics in the HERA Luminosity Upgrade Lattice of the Year 2000, *Proceedings of PAC (1999)*

[2] H. Grote, F. C. Iselin, The MAD program users's reference manual, Version 8.16, *CERN/SL/90-13 (AP) Rev. 4 (1995)*

[3] H. Mais and C. Mari, Introduction to Beam-Beam Effects, *DESY-M-91-4 (1991)*

[4] M. Sands, The physics of electron storage rings – an introduction, *SLAC-121 (1970)*

[5] Editor: U. Schneekloth, The HERA Luminosity Upgrade, *DESY-HERA-98-05 (1998)*

[6] D. Cocq, O. R. Jones, H. Schmickler, The Measurement of Chromaticity via a Head-Tail Phase Shift, *8th Beam Instrumentation Workshop BIW '98, SLAC (1998)*

[7] O. R. Jones, H. Schmickler, M. Wendt, F. Willeke, HEAD-TAIL Chromaticity Measurements at HERA-P (9/7/1998), *CERN Internal Note, SL Division (1998)*

[8] A. W. Chao, In Frontiers of Particle Beams, ed. by M. Month, S.Turner, Lect. Notes Phys., Vol.296 p.51 *(Springer, Berlin, Heidelberg (1988)*

[9] E. Gianfelice, Experience with a 90° optics, *Proceedings of the annual HERA Seminar, p. 144, (1998)*